

Jetlet Formation from Diabatic Forcing with Applications to the 1994 Palm Sunday Tornado Outbreak

DAVID W. HAMILTON, YUH-LANG LIN, RONALD P. WEGLARZ, AND MICHAEL L. KAPLAN

Department of Marine, Earth, and Atmospheric Sciences, North Carolina State University, Raleigh, North Carolina

(Manuscript received 5 November 1996, in final form 5 May 1997)

ABSTRACT

The three-dimensional responses of simple stably stratified barotropic and baroclinic flows to prescribed diabatic forcing are investigated using a dry, hydrostatic, primitive equation numerical model (the North Carolina State University Geophysical Fluid Dynamics Model). A time-dependent diabatic forcing is utilized to isolate the effects of latent heat release in a midlatitude convective system. Examination of the mass-momentum adjustments to the diabatic forcing is performed with a focus on the development of an isolated midlevel wind maximum. The results of both cases suggest the formation of a midlevel wind maximum in the form of a perturbation meso- β -scale cyclone, which later propagates downstream as the heating is decreased. The scale of the perturbation cyclone remains at a sub-Rossby radius of deformation length scale. Therefore, the mass perturbations adjust to the wind perturbations as the mesocyclone propagates downstream. Transverse vertical circulations, which favor ascent on the right flank of the wind maximum, appear to be attributed to compensatory gravity wave motions, initially triggered by the thermal forcing, which laterally disperses as the heating is reduced.

The simple model simulations are used to explain more complex results from a previous mesoscale modeling study (the Mesoscale Atmospheric Simulation System, MASS), in which it was hypothesized that an upstream mesoscale convective complex triggered a midlevel jetlet through geostrophic adjustment of the wind to the latent heat source. The MASS simulated jetlet attained a transverse vertical circulation that favored ascent on the right flank of the midlevel jetlet. The jetlet and accompanying transverse vertical circulations later propagated downstream aiding in the formation of the 27–28 March 1994 tornadic environment in Alabama and Georgia.

1. Introduction

The interaction of synoptic-scale and mesoscale motions is a subject of great interest to investigators. Particularly, scale interactions between deep convection and the synoptic airflow have been a major focus of much research during the last three decades (e.g., Fankhauser 1971; Maddox 1979; Anthes et al. 1982; Wolf and Johnson 1995). Many of these studies have focused their attention on how convection modifies the upper-tropospheric mass-momentum fields, particularly assessing the development of upper-level jet streaks (Maddox 1979). Interactions between upper-tropospheric jet streaks and convection have been addressed both observationally and with numerical models (Uccellini and Johnson 1979; Maddox et al. 1981; Anthes et al. 1982; Bluestein and Thomas 1984; Zack and Kaplan 1987; Wolf and Johnson 1995). Although these studies demonstrate cause and effect relationships between convection and upper-tropospheric jet streak features, the sub-

jects of 1) *midtropospheric* mass-momentum adjustments and 2) their influence on the synoptic airflow need further investigation. *It will be shown that deep convection may play a key role in not only developing and intensifying upper-tropospheric jet streaks but also initiating midtropospheric dynamical features that aid in severe weather development.*

A recent event has further revealed the complexity accompanying scale-interactive processes. During the early morning hours on Palm Sunday 27 March 1994 (hereafter PS94), numerous tornadoes were spawned across the southeastern United States by successive supercells that left 42 people dead, 320 others injured, and property damages that exceeded \$100 million. This event, on the synoptic scale, did not exhibit the “classic” features that often accompany such disastrous outbreaks. The absence of a well-defined surface low as well as little indication of an upper-level shortwave trough, kept forecasters limited to a “moderate risk” of a severe weather scenario well up until supercell development in central Alabama around 1500 UTC 27 March 1994 (Hales and Vescio 1996). Just prior to initial damage reports, the mesoscale environment was quickly modified (see Table 1 for a primary sequence of forecasted events). Subsynoptic datasets revealed the rapid

Corresponding author address: Dr. Yuh-Lang Lin, Dept. of Marine, Earth, and Atmospheric Sciences, North Carolina State University, Raleigh, NC 27695-8208.
E-mail: yl.lin@ncsu.edu

Table 1. Summary of Storm Prediction Center actions during the Palm Sunday tornado outbreak (26–27 March 1994) in Alabama and Georgia.

Date	Time (CST)	Product
26 Mar	2:00 A.M.	Day two outlook “Possibility of isolated supercells with a threat of tornadoes.”
26 Mar	Noon	Day two outlook “Some supercell tornadoes possible.”
27 Mar	1:00 A.M.	Day one outlook (“Moderate risk”—Alabama/slight risk—most of Georgia) “Primary threat of damaging winds; however, tornadoes are possible.”
27 Mar	9:05 A.M.	Mesoscale discussion for Alabama and Georgia “Possible tornado watch.”
27 Mar	9:18 A.M.	Tornado watch no. 41 valid until 4:00 P.M. (includes a large part of northern and central Alabama).
27 Mar	10:00 A.M.	Public severe weather outlook (includes much of Alabama and Georgia) “Potential for tornadoes, some could be intense.”
27 Mar	11:00 A.M.	Mesoscale discussion for Georgia “Very favorable wind structure for supercell/tornadic thunderstorms.”
27 Mar	11:47 A.M.	Status report watch no. 41 “Supercells moving across northern Alabama.”
27 Mar	12:00 P.M.	Tornado watch no. 42 valid until 8:00 P.M. (includes northern Georgia). “Particularly dangerous situation, very damaging tornadoes.”
27 Mar	1:20 P.M.	Status report watch no. 42 “Tornadic supercell Pickens County, GA.”
27 Mar	1:30 P.M.	Day one outlook (“High risk” for large part of Alabama and northern Georgia) “Numerous tornadic storms.”

development of a mesoscale environment capable of producing strong tornadic thunderstorms (Hales and Vescio 1996). These special datasets enabled forecasters to mark wind field inaccuracies in the models, reevaluate the stronger midlevel winds, and quickly update to a “high risk” scenario for a large part of Alabama and Georgia. The major question of this research is to investigate possible dynamical mechanisms necessary for the rapid development of the stronger midlevel winds that were observed during PS94.

Kaplan et al. (1998) conducted numerical simulations of PS94 with a hydrostatic mesoscale model (the Mesoscale Atmospheric Simulation System, MASS). It was hypothesized that convection triggered a midlevel *mesoscale jet streak* (hereafter “jetlet”) by the geostrophic adjustment of the atmosphere to the release of latent heat within the simulated storm complex far upstream of the outbreak. They claimed that the coarse rawinsonde network around the Texas–Louisiana border could not resolve the jetlet at 1200 UTC 27 March 1994, but it was shown that the jetlet was later detected by intermediate soundings and wind profilers around the time of the destruction of the Goshen United Methodist Church, in Cherokee County, Alabama, at 1739 UTC 27 March 1994. The simulated meso- β -scale midlevel (~ 500 mb) jetlet exhibited highly unbalanced leftward-directed ageostrophic winds throughout its exit region. Here, unbalanced refers to the direction of the transverse ageostrophic circulation accompanying the meso- β -scale jetlet, which is reversed from that known to preserve thermal wind balance of small Rossby number

synoptic-scale jet streaks. Such ageostrophy enabled a nearly continuous acceleration downstream, as well as an increase in midlevel mass divergence on the right flank of the jetlet. This resulted in the evacuation of mass from the underlying column on the right flank of the jetlet as it propagated over central Mississippi and into northern Alabama. This integrated mass loss enhanced the formation of a surface mesowall, the development of a low-level jetlet, as well as the eventual formation of an environment that was capable of producing and supporting the simulated deep convection (Kaplan et al. 1996; Koch et al. 1996). It appears that a phenomenon capable of organizing deep convection, such as this jetlet, can form on temporal and spatial scales smaller than what can be resolved by the normal rawinsonde network. Thus, a numerical study is important in examining such a possible unresolvable feature.

Maddox (1979) and others have examined mesoscale convective systems (hereafter MCSs) to understand their role in the modification of upper-level dynamics, with emphasis on upper-tropospheric jet stream intensification. The term MCS describes a large deep convective system often marked by a broad and persistent middle- to upper-tropospheric stratiform region (Cotton and Anthes 1989). These studies discuss midtropospheric warming associated with convective latent heat release, but seem to omit the responses of the momentum field at *midlevels*. On the other hand, Fankhauser (1971) has performed a well-documented observational investigation into the role of airflow modification in the vicinity

of an MCS, and found the development of midlevel wind maxima on either side of the thunderstorm tower. He claimed that blocked flow, similar to quasi-potential flow around a cylinder, was the physical mechanism responsible for producing the flanking wind maxima. However, he failed to comment on the effects of convective latent heating as a contribution to the development of the storm flank maxima.

The emphasis in the present research is to investigate the role of convective latent heating on background mid-level flow modification and determine its contribution to the development of an environment favorable for severe weather downstream from the latent heat source. A prescribed diabatic forcing in a simple three-dimensional primitive equation model (Weglarz 1994; Lin and Jao 1995; Wang et al. 1996) appears to be useful to represent latent heat release experienced in the real atmosphere during deep convective events. Theoretical studies (Lin and Smith 1986; Lin 1986; Lin and Li 1988) have shown that a prescribed diabatic forcing representing convective latent heating can produce observable properties of meso- γ -scale convection. Replication of features associated with simple cumulus convection generated by impulsive and steady heating is achieved in these studies. These studies show that the parameterization of prescribed thermal forcing was useful in determining that latent heat release can act as a source mechanism for gravity wave generation near the top of the heating region, producing the formation of the V-shaped cloud-top signature often observed in the anvil of severe supercell storms (e.g., Fujita 1982; Heymsfield 1983). A similar approach will be adopted here, and furthermore appears to be useful for studying the modification of mesoscale environments by the existence of deep convection.

As far as it is known to the authors, there has been little investigation into the role of latent heat release on background hydrostatic midtropospheric mass-momentum adjustments at sub-Rossby radius of deformation length scales. The present study examines meso- β -scale disturbances caused by latent heating focusing on the midlevel response to latent heating and its implication for downstream environmental modification. An idealized numerical investigation appears to be a key step in isolating the effects of latent heat release and examining such phenomena.

In the present study, the role of latent heating on the development of a midlevel local wind maximum and accompanying downstream mass-momentum adjustments is examined. Observational evidence and mesoscale model results from Kaplan et al. (1996, 1998) support the development of a midlevel jetlet by geostrophic adjustment of the wind to the mass field accompanying the latent heat release of an MCS in east Texas, early on the day of 27 March 1994. The jetlet later propagates downstream and through its own mass-momentum adjustments yielded transverse vertical circulations that favored the development and maintenance

of deep convection over Alabama and Georgia (Kaplan et al. 1996, 1998). This case study has led to the concept of the relative importance of latent heat release within MCSs in significantly modifying the downstream environment so that it may favor the development of severe weather. Review of the literature reveals a major gap in our understanding of the midlevel wind structure modifications triggered by latent heat release.

A simple, idealized, three-dimensional numerical model is used to isolate the role of the latent heating within an MCS. We examine its effects on the surrounding environment, with emphasis on midlevel adjustments, in order to easily explain the findings of Kaplan et al. (1996, 1998). Vertical motion patterns attendant to the responding midtropospheric flow will be examined to determine any modifications that might prove favorable for the development of severe weather. Section 2 will briefly review the MASS model-simulated atmospheric structure on 27 March 1994 in order to understand the evolution of the MCS that triggered the simulated mesoscale jetlet. In addition, we will examine the corresponding vertical circulations associated with the jetlet. In section 3, we will employ the idealized model to determine whether or not the effects of latent heat release on the surrounding environment aids in the formation and development of the midlevel jetlet and corresponding flow modifications, which may be favorable for the subsequent development of severe weather. A primitive equation model will be implemented with a prescribed heat source to examine the problem. This model will provide insight to the dry hydrostatic dynamical response to prescribed diabatic forcing without the addition of complexities contributed by moist thermodynamical and boundary layer processes. Simulated features will be compared with observed convection for verification of the prescribed forcing, as well as the identification of a midlevel wind maximum. A discussion of this study and possibilities for future work will be addressed in the final section.

2. Review of three-dimensional full physics model simulation of a mesoscale jetlet during the Palm Sunday tornado outbreak

Kaplan et al. (1996, 1998) used MASS (Kaplan et al. 1982) to simulate the mesoscale environment conducive to the 27 March 1994 Palm Sunday tornado outbreak. We will briefly review the simulated development of convection in eastern Texas and the resultant triggering and evolution of the midlevel jetlet, which occurred around the forecasted time of 1200 UTC 27 March 1994. The convection is examined to determine a representative latent heating profile for initialization of the idealized numerical model in section 3. After examination of the midlevel jetlet evolution we will employ the idealized numerical model study to provide simple explanations for the observed unbalanced midlevel flow as discussed by Kaplan et al. (1996, 1998).

A vertical cross section from a fine-mesh simulation valid at 0700 UTC March 1994 is shown in Fig. 1a and reveals the region of convective initiation in central Texas. Around 850 mb, negative Richardson numbers and overturning of the isentropes indicate superadiabatic lapse rates. Simulated convection erupts within this region and strengthens as it propagates toward the Texas–Louisiana border, where the larger-scale environment was shown by Kaplan et al. (1996, 1998) to be favorable for the formation of deep convection. Figures 1b and 1c are the radar summaries at 0635 and 0735 UTC 27 March 1994 and reveal the observed convection in central Texas.

The coarse-mesh simulated 9-h 500-mb forecast valid at 0900 UTC 27 March is shown in Figs. 2a and 2b. In Texas, convection is evident by the shaded region of latent heat release (Fig. 2b). As the convection rapidly evolves, the height field is perturbed so that an evolving region of subgeostrophy, attaining a significant leftward-directed ageostrophic wind component, becomes apparent (Fig. 2b). It has been shown for a straight jet streak that the geostrophic momentum approximation

$$\frac{D\mathbf{V}_g}{Dt} = -f\mathbf{k} \times \mathbf{V}_a, \quad (1)$$

where

- \mathbf{V}_g = geostrophic wind vector,
- \mathbf{V}_a = ageostrophic wind vector,
- \mathbf{k} = vertical unit vector in Cartesian coordinates, and
- f = Coriolis parameter,

describes the geostrophic acceleration of air parcels by their ageostrophic components. Therefore, Eq. (1) dictates that the winds must adjust by accelerating the flow in that region. By 1100 UTC, winds of 40 m s^{-1} are evident (Fig. 2c) as well as the intensified regions of subgeostrophy on the downstream flanks of enhanced latent heat release (Fig. 2d) where ageostrophic winds in excess of 50 m s^{-1} are directed across and against the geostrophic flow.

Over the next few hours the convection in Texas regenerates and propagates into northern Louisiana and southern Arkansas, thus providing a continuous supply of latent heat to the simulated midlevel atmosphere. Similar to a wave–CISK mechanism (e.g., Raymond 1976), as the convection is continuously driven at lower levels, latent heat release continues to establish this adjustment of the wind to the mass field. Therefore, a quasi-continuous geostrophic adjustment maintains and intensifies the jetlet at midlevels.

A vertical cross section of the coarse-mesh simulation, at 1400 UTC—from New Orleans, Louisiana (MSY), to Pine Bluff, Arkansas (PBF)—passing through the core of the midlevel jetlet, is shown in Fig. 3a, and reveals the associated transverse ageostrophic flow and vertical motions about the jetlet. The transverse ageostrophic circulation vectors roughly describe the

perturbations associated with the jetlet and will be used for comparison with the perturbation fields accompanying the Geophysical Fluid Dynamics Model (GFDM) idealized jetlet. Shaded regions are isotachs, clearly showing the jetlet around the 400-mb level. To the north, the shaded regions depict the preexisting polar jet entrance region (Fig. 2c). The convection triggering the jetlet is apparent between the two wind maxima and is delineated by both the ageostrophic wind barbs and omega field with upward motion exceeding $-48 \mu\text{b s}^{-1}$. *The important point here is to delineate the circulations about the midlevel jetlet. These circulations will be compared with similar simpler circulations in the idealized simulations, which are hypothesized as being favorable for the downstream triggering of convection.* Just below the jetlet, a nearly closed thermally direct circulation can be delineated, with a similar but opposing thermally indirect circulation above the jetlet located just to the south but affixed to the lower circulation. This feature, as delineated by the wind vectors in Figs. 3a–c, takes on an S-shape vertical motion pattern with air generating from the bottom of the “S.” Consequently, an ascending branch is developed beneath the jetlet, denoted by the ascending nose of upward motion transfixed between the two descending layers located just to the north and south of the region of the maximum midlevel winds. This feature remains quasi-steady over the next 5 h and is further addressed in Figs. 3b and 3c, which are similar vertical cross sections—one from Pensacola, Florida (PNS), to Memphis, Tennessee (MEM), and the other from Columbus, Georgia (CSG), to Owensboro, Kentucky (OWB)—constructed 2 and 4 h after the one depicted in Fig. 3a, respectively. The ascent below the midlevel jet later triggered convection over northern Alabama and Georgia (Kaplan et al. 1996, 1998).

In summary, numerical simulations by Kaplan et al. (1996, 1998) indicate a tropospheric sequence of events on 27 March 1994 that include the development of a large MCS over eastern Texas, which was observed early on 27 March 1994. Subsequently, the convection perturbs the midlevel pressure field so that a region of intense leftward-directed subgeostrophic wind velocities develops, forcing the winds to compensate for the increased pressure gradient forcing on the right flank of the simulated convection. Thus, the midlevel jetlet feature is produced and is reinforced by the continual growth and reformation of convection. This results in a continuous acceleration of the winds near the level of maximum heating and the eventual enhancement of the unbalanced jetlet. The wave–CISK process provides the mechanism for the downstream propagation of the simulated convection and the midlevel jetlet. Maintenance of the latent heat release by the wave–CISK process is necessary for the continual intensification of the midlevel jetlet, which will also be shown to be true of midlevel wind anomaly evolutions to be presented in the simpler idealized model simulations in section 3. Ageostrophic vertical circulations below the responding mid-

level jetlet enable a secondary ascending branch of air to develop below and to the south of the jetlet. This secondary ascending branch is a part of a nearly closed thermally direct circulation, which is maintained for approximately 6 h as it propagates over northern Alabama. The low-level secondary vertical motions, associated with the midlevel jetlet, aid in the formation of an environment capable of triggering convection downstream. Therefore, they will be examined in the following section to provide a simple explanation for their development.

3. Flow response to deep, elevated meso- β -scale diabatic heating

In this paper, we hypothesize that MCSs *not only aid in the development of upper-level mass-momentum adjustments, but that midlevel mass-momentum adjustments can provide the mechanism for the formation of a midlevel jetlet and the downstream development of an environment capable of producing severe weather*. The purpose of this section is to examine the effects of a simple prescribed diabatic forcing on midlevel wind anomalies and their subsequent influence on the downstream environment to simply explain features discussed in section 2. The prescribed heating function chosen here is representative of the latent heating profiles taken from the MASS model simulations of PS94 (Kaplan et al. 1996, 1998). This is necessary for valid comparison of the mesoscale midlevel flow modifications between the MASS simulated MCS over Texas and the idealized convection examined in this paper.

We will present the results of two cases, each utilizing the same forcing function and magnitude, which are described below. For simplicity, the first case will investigate the response of a uniform barotropic flow to the diabatic heating. This will provide insight into the simple atmospheric responses to the prescribed thermal forcing, which will become more complicated when the second case is examined. The second case investigates the more complex response of a baroclinic shear flow. The shear case is more representative of the actual atmospheric adjustments to a diabatic heat source. The shear profile is simplified from the LCH observed sounding at 1200 UTC 27 March 1994. This sounding was most appropriate for the experiment since it was the nearest rawinsonde report to the development of convection in eastern Texas on 27 March 1994.

a. Model description

The North Carolina State University (NCSU) GFDM is adopted for the simulations conducted in this study. It is a dry hydrostatic model in terrain-following coordinates based on the three-dimensional nonlinear primitive equations governing diabatically and orographically forced finite amplitude perturbations in a continuously stratified, Boussinesq atmosphere on a

planetary β plane. Since there exists no terrain in these simulations, the grid will reduce to a uniform structure.

The details of the numerical model can be found in Weglarz (1994), Lin and Jao (1995), and Wang et al. (1996). The basic wind (U) is assumed to be independent of x , y , and σ in the barotropic case, but linearly increases with height in the baroclinic case. The Brunt-Väisälä frequency associated with the basic flow is assumed to be 0.01 s^{-1} for all experiments discussed in this study. Coriolis effects are included in the model by making an f -plane approximation. The reference Coriolis parameter f_o is set to $7.292 \times 10^{-5} \text{ s}^{-1}$, corresponding to a latitude of 30°N , which is the approximate location of jetlet formation in the MASS model. The flow is assumed to be inviscid in the physical domain (i.e., $z \leq 15 \text{ km}$). The vertical grid interval is 500 m, while the horizontal grid interval in both x and y directions is 10 km. The total number of model grid points in the x , y , and σ directions are $64 \times 64 \times 31$, respectively.

b. A prescribed thermal forcing

Initialization of a time-dependent diabatic forcing is designed from the analysis of the MASS simulated latent heating profiles. The latent heat release in the MASS simulations is difficult to explicitly extract due to the regenerating nature of multicell convection (Fig. 2). Therefore, a simple mathematical function is prescribed to replicate one selected cell from the MASS simulation. By using the simple relation of the local temperature tendency and the diabatic heating term in the thermodynamic equation, the maximum heating rate is estimated as $2.8 \text{ J kg}^{-1} \text{ s}^{-1}$. The steady-state heating distribution (from which the time-dependent function is built) is defined as

$$Q_o(x, y, z) = \frac{Q_m}{[(x - x_{qc})^2/b_x^2 + (y - y_{qc})^2/b_y^2 + 1]^{3/2}} \times \exp\left\{-\frac{(z - z_c)^2}{b_z^2}\right\}, \quad \text{for } z_b \leq z \leq z_t, \quad (2)$$

where

$$\begin{aligned} Q_o(x, y, z) &= \text{spatial heating distribution;} \\ Q_m &= \text{maximum latent heating rate (J kg}^{-1} \text{ s}^{-1}\text{);} \\ x_{qc}, y_{qc} &= \text{heating center;} \\ b_x, b_y, b_z &= \text{half-widths of the cumulus heating in } x, y, \text{ and } z \text{ directions, respectively;} \\ z_c &= \text{height of heating center;} \\ z_b &= \text{base of heating;} \text{ and} \\ z_t &= \text{top of heating.} \end{aligned}$$

In this study, the parameters used are $Q_m = 2.8 \text{ J kg}^{-1} \text{ s}^{-1}$, $x_{qc} = y_{qc} = 0 \text{ km}$, thus indicating that the thermal

forcing is at all times located at the center of the computational domain, $b_x = b_y = 40$ km, $b_z = 2.5$ km, $z_b = 1$ km, $z_c = 5.5$ km, and $z_t = 10.5$ km. A comparison of the extracted latent heat release from the MASS model and the prescribed latent heating, in dimensions of $\text{K} (30 \text{ min})^{-1}$, is given in Fig. 4. The heating is set to zero above and below the assumed cloud top (~ 10.5 km) and bottom (~ 1 km), respectively.

Wolf and Johnson (1995) studied the time evolution of latent heat release from a simulated MCS, and it was found that over a 12-h life span of the storm, the diabatic forcing dominated at the sixth hour. It should be noted that in the MASS simulation a cluster of convective cells persists for at least a 12-h period as the cluster propagates northeastward from eastern Texas to western Tennessee. Time-dependent heating is obviously much more realistic in simulating MCS evolution (Wolf and Johnson 1995). Therefore the inclusion of a time-dependent heating should be more representative of the MASS simulated latent heat release as well as that associated with real MCSs and is taken to be

$$Q(x, y, z, t) = Q_o(x, y, z) \left[1 - \cos\left(\frac{\tau - t}{\tau} \pi\right) \right], \quad (3)$$

for $0 \leq t \leq 12$ h,

where

$Q(x, y, z, t)$ = time-dependent heating distribution

and

τ = total timescale (12 h).

The time-varying heating function aids in reducing any shock to the numerical model and will better rectify the actual modification of the near-storm environment. The simulation is performed for a total integration of 12 h, with heating set to zero at $t = 0$ and 12 h with maximum heating occurring at $t = 6$ h.

c. Response of a uniform, continuously stratified barotropic flow

We will begin with the 6-h response, which corresponds to the time of maximum heating. The near-surface fields reveal a V-shaped pattern indicative of a downward-propagating gravity wave, which is apparent at and below the base of the thermal forcing. In Fig. 5a, the 6-h forecast at the 500-m level shows a vertical velocity maximum at about 60 km upwind of the thermal forcing and downward motion located just downwind. The downdraft, located to the rear of the forcing, is in

the shape of a “W” (Fig. 5a) and is associated with the compensating downdraft for the rising motion just to the west. The ascent region is out of phase due to the upstream propagation of the thermally forced gravity wave. As one would expect in regions of latent heat release during deep convection, the updraft becomes more in phase with the prescribed heating as one moves aloft to the cloud base and to higher levels. Figure 5b shows the vertical velocity, which at 9 km remains positive and in phase with the heating, although a small area of descent appears to be developing just downstream. Above the heating top a vertically propagating gravity wave is apparent (Fig. 5c).

The prescribed heating enables both upward and downward vertically propagating waves to propagate away from the forcing region and allows the air parcel to pass through the forcing region. Lin and Smith (1986) examined the two-dimensional responses of a stratified fluid flow to pulse and steady heating. They discuss the concept that continuous heating acts as a superposition of an infinite number of individual elements corresponding to individual pulses of heat separated by infinitesimal time intervals. Initially, the heating can be considered as a single disturbance triggering an individual wave. This initial wave is allowed to propagate away from the pulse source. Continuous heating, acting as numerous pulses of heat, triggers continuous waves. Therefore, the initial wave disturbance appears to grow with time as the total number of waves become superimposed, somewhat masking the propagation of the initial wave mode. This leads to the appearance of two wave modes. The first is a stationary mode of upward motion, which stays in the vicinity of the wave generation region or the region of thermal forcing and has a weak compensating downward motion. It is indicated as the stationary mode since the elevated heating is prescribed and remains stationary at the origin. The second is a propagating mode, indicating the propagation of the superimposed waves. These modes will be referred to later when lateral dispersion of the thermally forced gravity wave becomes more apparent as the heating decreases after 6 h.

The quasi-V-shaped patterns are associated with the upward propagation of the gravity wave triggered by the heating, similar to that found for flow over mesoscale mountains (Smith 1980). Smith (1980) found that vertically propagating gravity waves are generated for three-dimensional flow over a bell-shaped mountain, and take the form of parabolas with the vertex facing upstream. Downstream propagation of this wave, having a slower phase speed than that of the basic current, aids

←

FIG. 1. (a) MASS simulated fine-mesh vertical cross section valid at 0700 UTC 27 March 1994 of Richardson numbers (thick solid and dashed below 0.25), relative humidity (dotted) $> 70\%$ shaded every 10%, cross ageostrophic circulation (vectors), and potential temperature (thin lines). Cross section is depicted in Fig. 2b. National Meteorological Center (now known as the National Centers for Environmental Prediction) radar summaries on 27 March 1994 at (b) 0635 and (c) 0735.

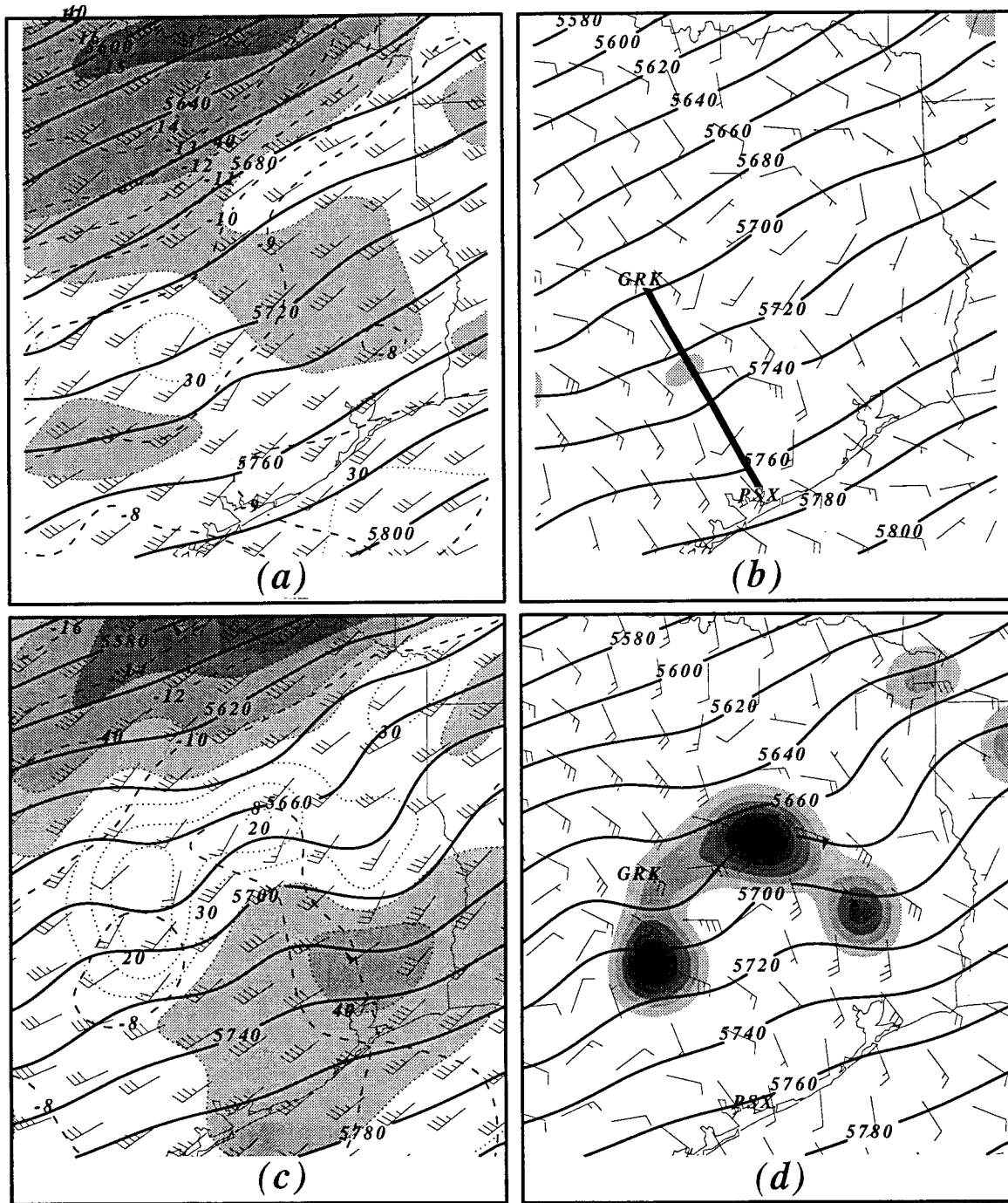


FIG. 2. MASS-simulated coarse-mesh upper-air plots of 500-mb valid at (a) and (b) 0900 UTC and (c) and (d) 1100 UTC 27 March 1994. In (a) and (c) winds $> 35 \text{ m s}^{-1}$ shaded every 5 m s^{-1} , and simulated total wind barbs in m s^{-1} . In panels (b) and (d) latent heat release $> 2 \text{ K (30 min)}^{-1}$ shaded every $2 \text{ K (30 min)}^{-1}$, and simulated ageostrophic wind barbs in m s^{-1} . Heights (m) are denoted by solid lines.

in the development of a V-shaped signature (Lin and Li 1988).

The horizontal winds at 500 m reveal the development of an isolated wind maximum that is located upstream of the heating region and coupled with a minimum re-

gion downstream, indicating thermally induced convergence upstream of the heating base (Fig. 6a). The v' component also exhibits a similar pattern of convergence, but is not shown. The thermal forcing hydrostatically imposes a low pressure perturbation below the

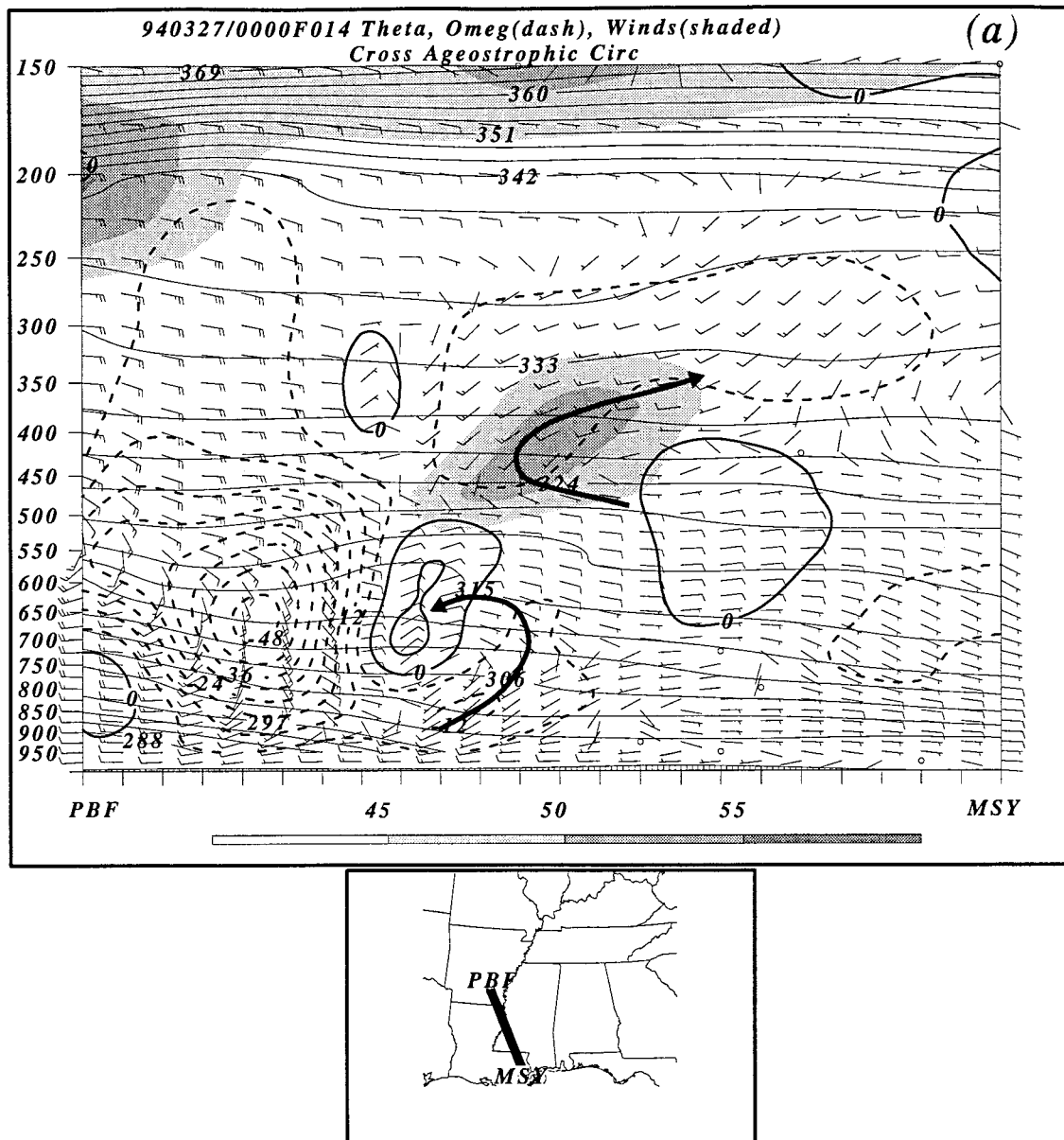


FIG. 3. MASS-simulated coarse-mesh vertical cross sections for (a) Pine Bluff, AR (PBF), to New Orleans, LA (MSY), valid at 1400 UTC 27 March 1994; (b) Memphis, TN (MEM), to Pensacola, FL (PNS), valid at 1600 UTC 27 March 1994; and (c) Owensboro, KY (OWB), to Columbus, GA (CSG), valid at 1800 UTC 27 March 1994. Simulated isotachs $> 50 \text{ m s}^{-1}$ shaded every 5 m s^{-1} , potential temperature (K) are thin solid lines, omega ($\mu\text{b s}^{-1}$) are thick solid and dashed lines, and wind barbs are the cross ageostrophic circulation in m s^{-1} .

level of maximum heating. The resultant pressure gradient force drives horizontal convergent motion toward the low pressure center, which in turn triggers vertical motions through continuity. Moreover, the diabatic forcing acts to induce an initial distribution of positive potential vorticity in the lower levels (Weglarz 1994). As the vertical motions develop, stretching of the vortex tubes intensifies the cyclonic vorticity below 6 km. At 5 km, a maximum in the u' component of almost 4 m s^{-1} is apparent (Fig. 6b) and is also located upstream

from the heating. Moving upward to 9 km, a reversal in the horizontal wind pattern is apparent and exhibits divergence associated with the evacuation of the updraft core (Fig. 6c). This pattern reveals an upper-tropospheric wind maximum on the left-forward flank of the heating and agrees with previous observations and modeling results (Maddox 1979; Maddox et al. 1981; Wolf and Johnson 1995).

The mass field at 6 h also details observable qualities of ensembles of convective storms. As expected, in the

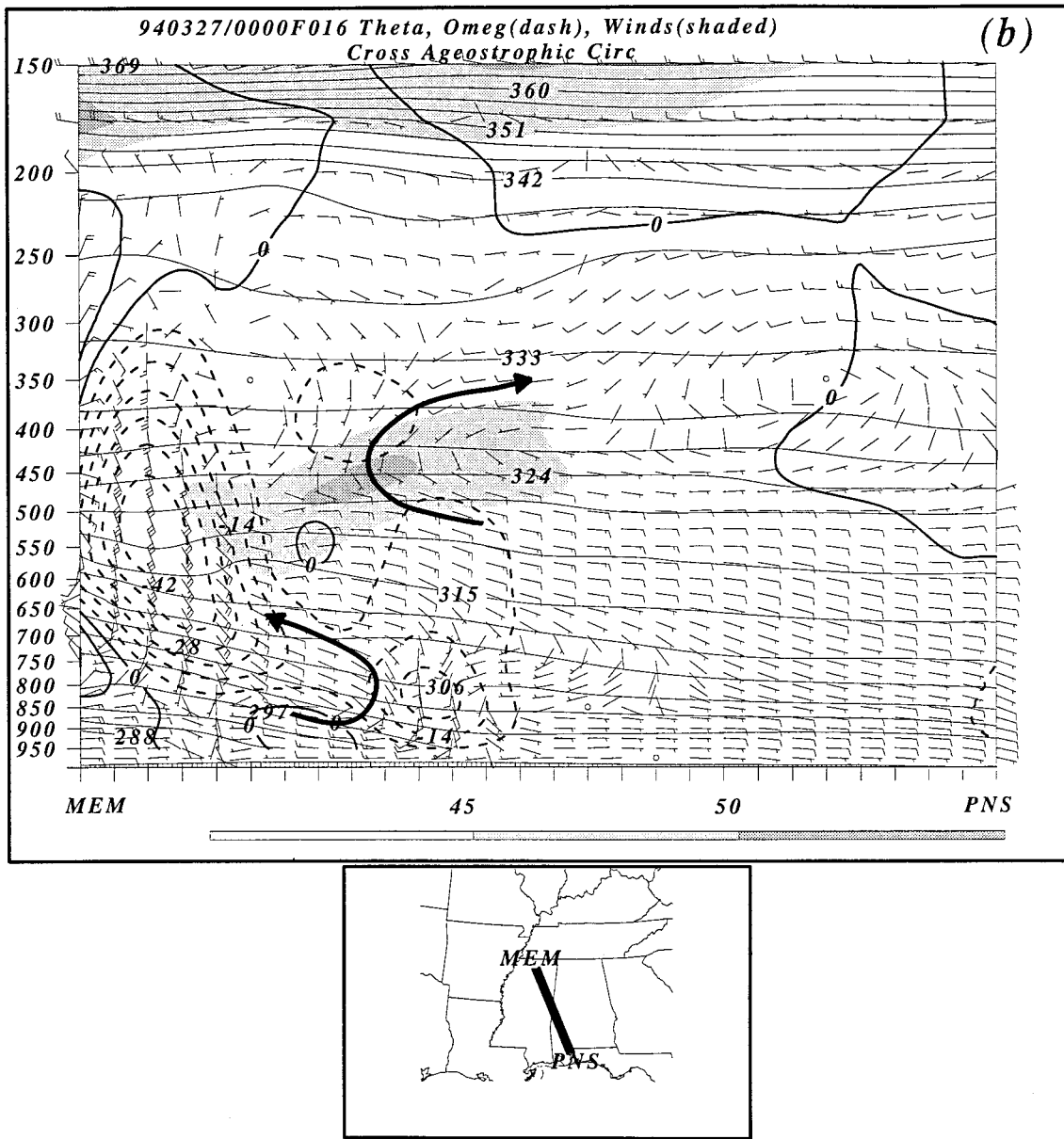


FIG. 3. (Continued)

lower and middle troposphere, the hydrostatic response exhibits a low pressure center below the heat source (not shown). Conversely, a positive pressure perturbation is located above the level of maximum heating. The influence of the positive pressure perturbation aloft acts to drive the upper-tropospheric divergence discussed in the previous paragraph. In Fig. 7, the adverse pressure gradients, located to the rear of the heating region, aid in upstream deceleration of the winds, leading to a blocking effect (Fankhauser 1971), whereas strong streamwise pressure gradient forcing assists in the acceleration due east of the heating region. The latter accelerating flow is similar to previous findings of accel-

erated upper-tropospheric momentum fields downstream of convection (Maddox 1979; Maddox et al. 1981).

The previous discussion can also be extended to explain the adjustment of the wind field when exposed to a diabatic heat source, as well as the results of Kaplan et al. (1996, 1998). The comparison of the effects of the heating between GFDM and the MASS simulation is given in Fig. 8. The effects of latent heat release in the MASS simulation is difficult to explicitly resolve, therefore a simulation where latent heat was suppressed is used to examine its effect. Figure 8a is the MASS simulated pressure gradient force difference, tangential to the cross section, between the full physics and the

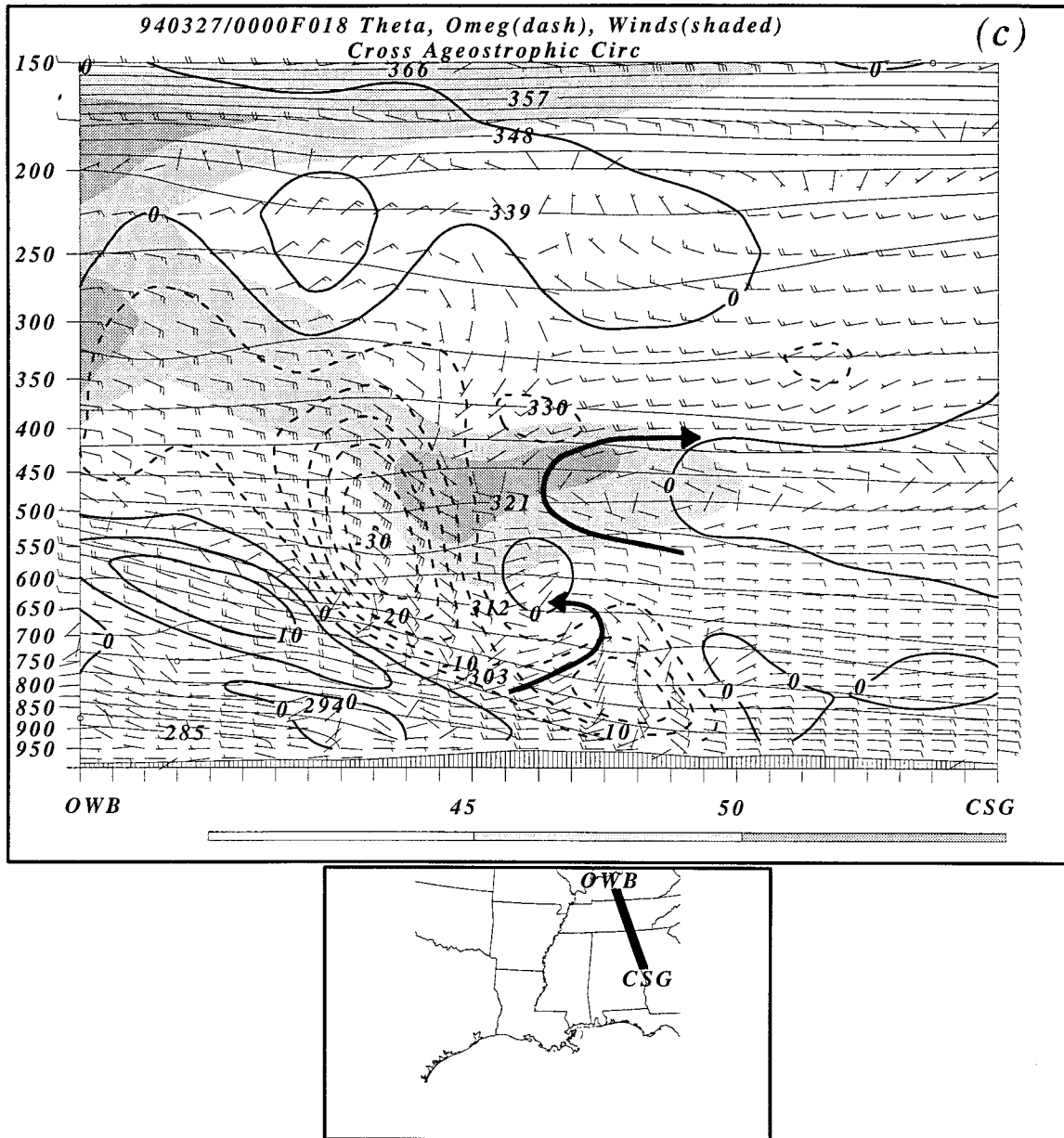


FIG. 3. (Continued)

suppressed latent heating simulations. The case with no latent heating is subtracted from the heating case as this will aid in removing the background pressure gradient force. It appears that the heating induces both convergence and divergence by pressure gradient forcing below and above the level of maximum heating, respectively. Though the magnitude in the MASS run is roughly three times less than that simulated by GFDM it is qualitatively consistent with the response of the zonal perturbation winds in GFDM. Figure 8b reveals similar divergence patterns in response to the prescribed heating.

For the final 6 h of simulation, the prescribed heat source is decreased and is terminated at 12 h. The most notable features to be discussed are 1) the decay of the updraft, 2) the development of a midlevel meso- β -scale cyclone (hereafter mesoscale cyclone) that propagates downstream, 3) the maintenance and downstream advection of weakening vorticity, and 4) the dispersion of the thermally forced gravity waves.

After 6 h, the updraft begins to decay. Ascent between 3 and 9 km is maintained by convergence in that layer. Cotton et al. (1989) revealed that during the mature stage of an MCC, deep midlevel mesoscale convergence

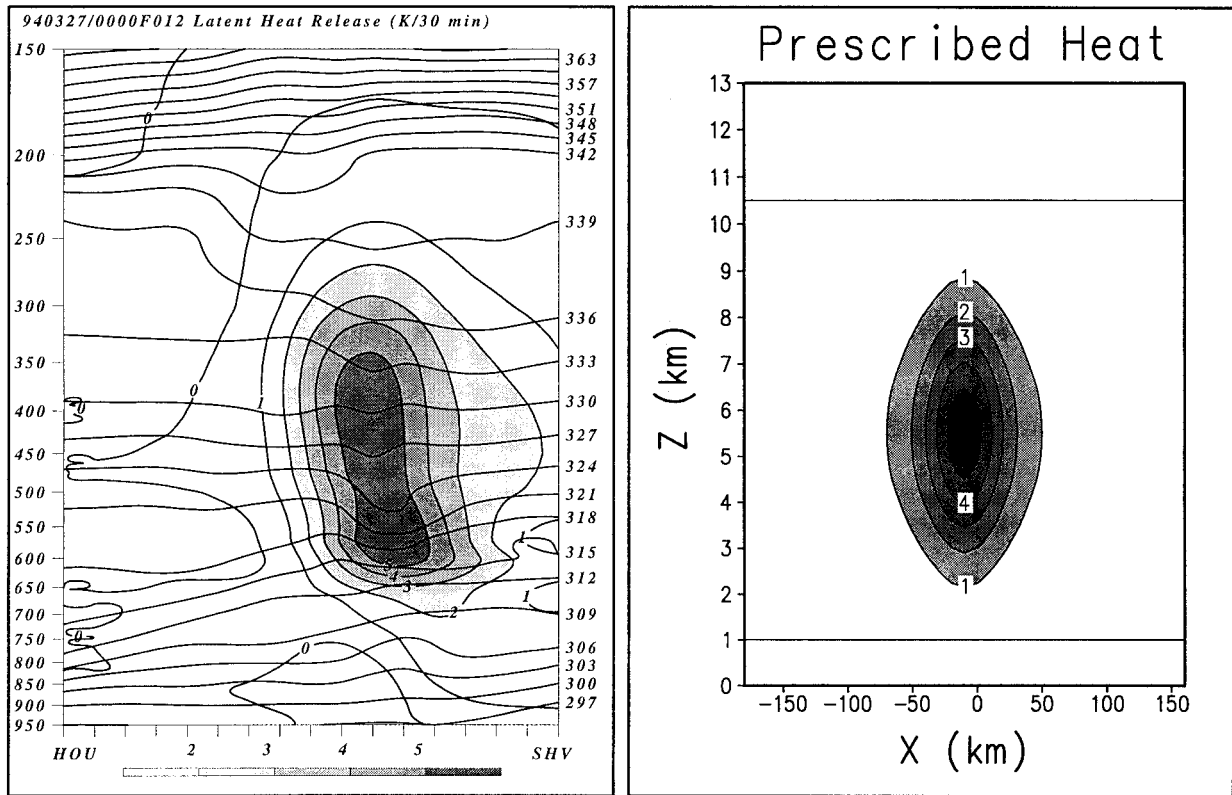


FIG. 4. Heating rates from (a) MASS simulation [K (30 min)⁻¹, one horizontal tick mark ≈ 20 km] and (b) prescribed in GFDM [K (30 min)⁻¹].

aids in sustaining the MCC. At 9 km, the updraft core begins to decay while the coupled downdraft (Fig. 5b) increases in size and magnitude.

As the heating decays, a very interesting feature develops. The positive zonal wind perturbation upstream of the heating region at 3 and 5 km appears to rotate cyclonically about the prescribed forcing region as the rotational force becomes important (Fig. 9a). This results in a right flank wind maximum that develops near the region of maximum heating (6 h), then bifurcates away from the convergent core and propagates downstream as the heating is decreased. At midlevels (e.g., 5 km) successive hourly plots reveal the downstream movement of the isolated zonal wind maximum that is countered with a return minimum to the north of the heat source. It is important to note, however, that this mesoscale cyclone attains a closed circulation in the perturbation fields, but appears as an open wave in the total wind field (Fig. 11b) with winds exceeding 12 m s⁻¹. A closed low pressure perturbation is identifiable at 5 km (Fig. 9b), which is collocated with a positive potential temperature perturbation (Fig. 9c) within the mesoscale cyclone. Interestingly, the mesoscale cyclone, at 5 km, continues to intensify as it moves downstream and reaches a maximum positive wind perturbation of nearly 3 m s⁻¹ by 12 h (Fig. 9a). In a sensitivity experiment in which the model's rotation was sup-

pressed (i.e., $f = 0$), the mesoscale cyclone did not form. This clearly indicates the importance of rotation and, hence, the geostrophic adjustment process on the formation of the mesoscale cyclone and, moreover, the local wind maximum. This feature is evident at 3 km but is not as intense. At 9 km, a warm core intensifies in the final 6 h, and is attributed to the intensification of the downstream region of descent depicted in Fig. 5b. As this region increases in size and magnitude, persistent adiabatic compression influences the formation of the warm core.

It appears that the evolution of the mesocyclone feature is partially caused by the existence of the two wave modes described earlier. At 6 h, the stationary mode, or the region of maximum convergence, is evident at the origin. Later, as the heating decays, the propagating mode becomes apparent by the downstream movement of the perturbation mesoscale cyclone as well as the upstream propagation of an inertia-gravity wave (Fig. 9a). This feature is largely evident due to the dominant wave amplitude that was triggered by the maximum heating at 6 h. After 6 h, reduced heating decreases the amplitude of each wave that is triggered thereafter, thus contributing to the unmasking of the upstream and downstream propagating modes (Fig. 10).

Figure 10 is a time-height graph revealing the existence of these two wave modes. At 6 h, the peak heat-

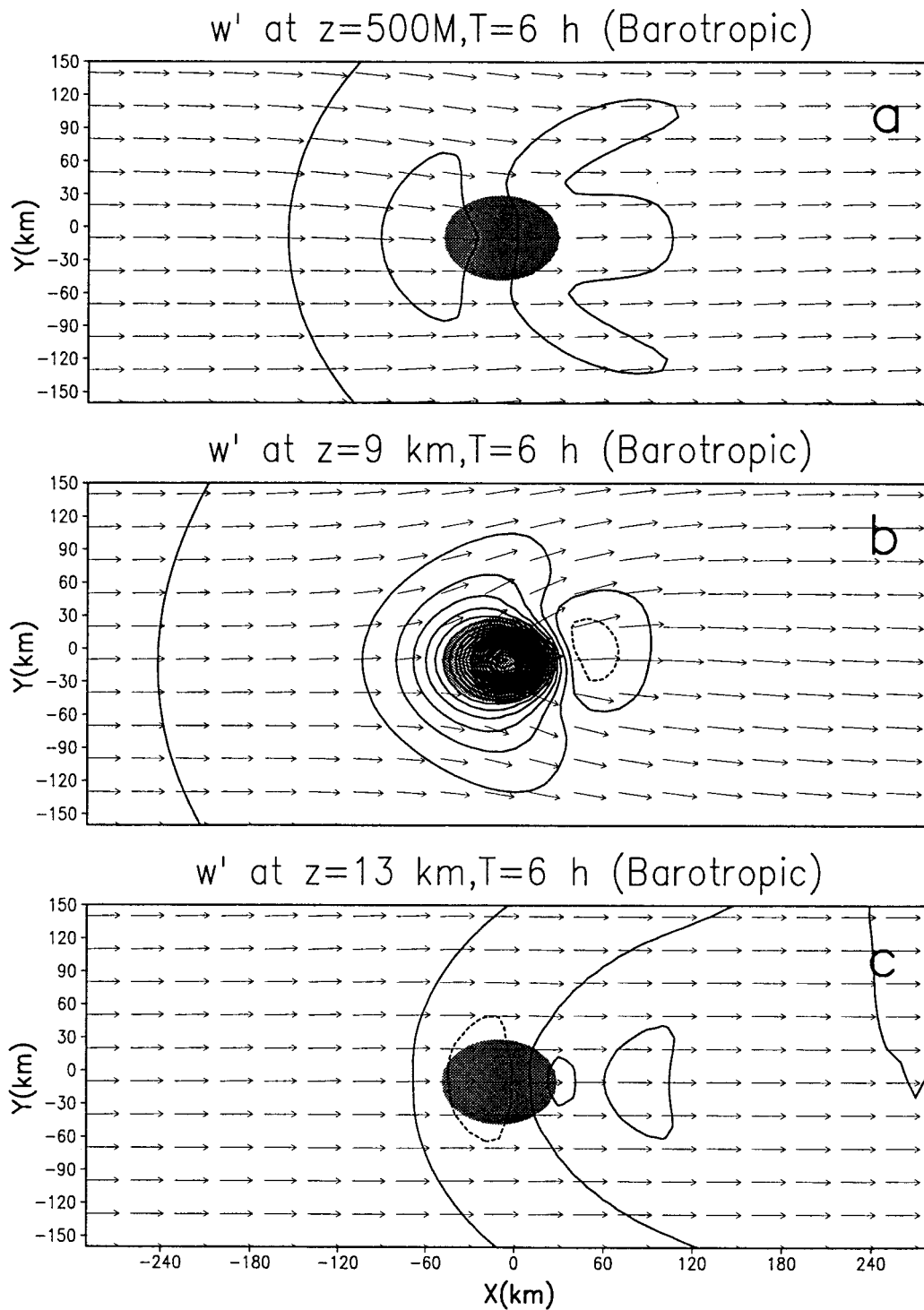


Fig. 5. Vertical velocity (contoured every 0.02 m s^{-1}) and total horizontal wind vectors for the barotropic case at $t = 6\text{ h}$ and (a) $z = 500\text{ m}$, (b) $z = 9\text{ km}$, and (c) $z = 13\text{ km}$. Heating rate $> 1\text{ W kg}^{-1}$ at $z = 5\text{ km}$ is shaded.

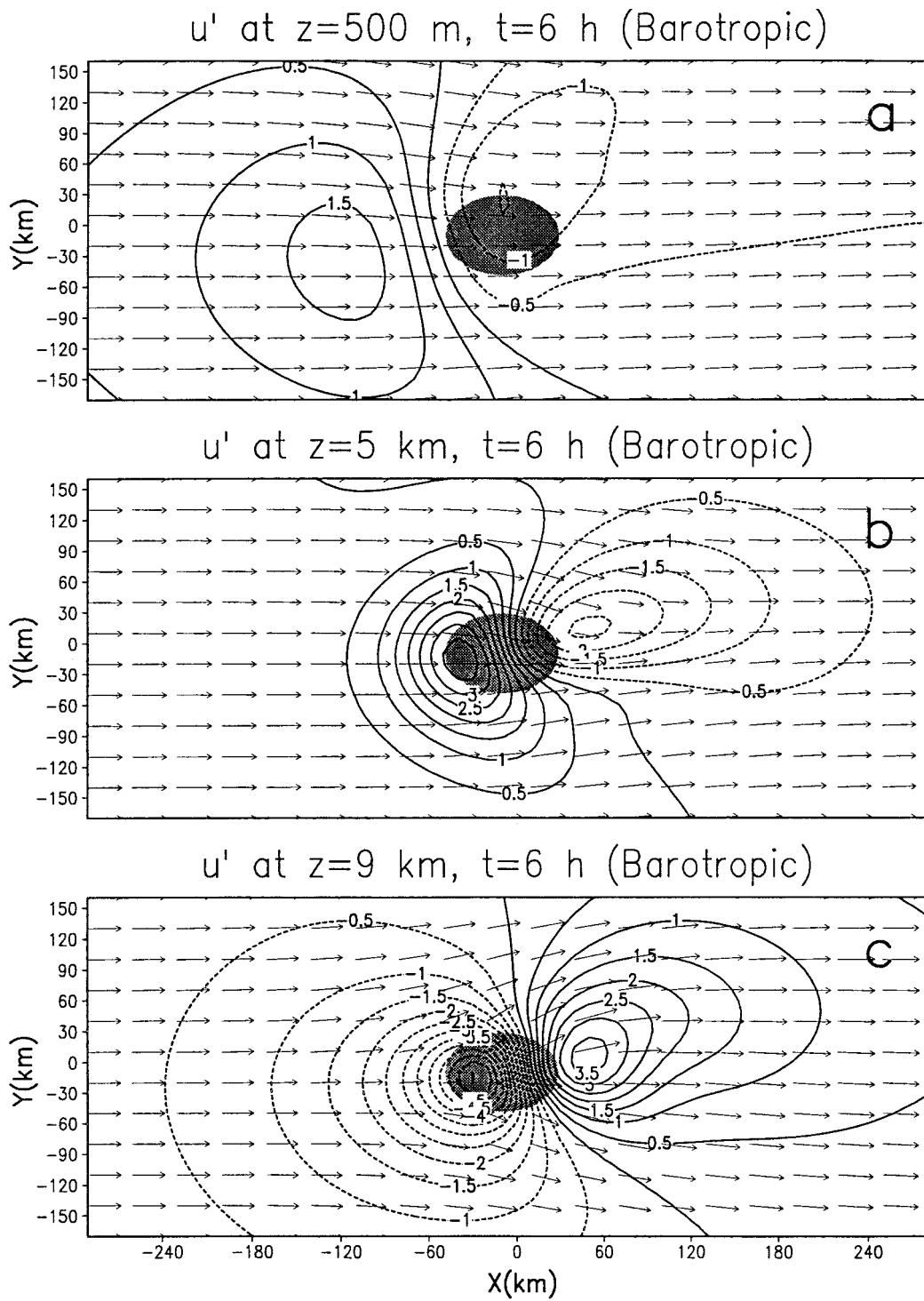


FIG. 6. Horizontal zonal wind component (u') and total horizontal wind vectors for the barotropic case at $t = 6$ h and (a) $z = 500$ m, (b) $z = 5$ km, and (c) $z = 9$ km. Shading is the same as in Fig. 5.

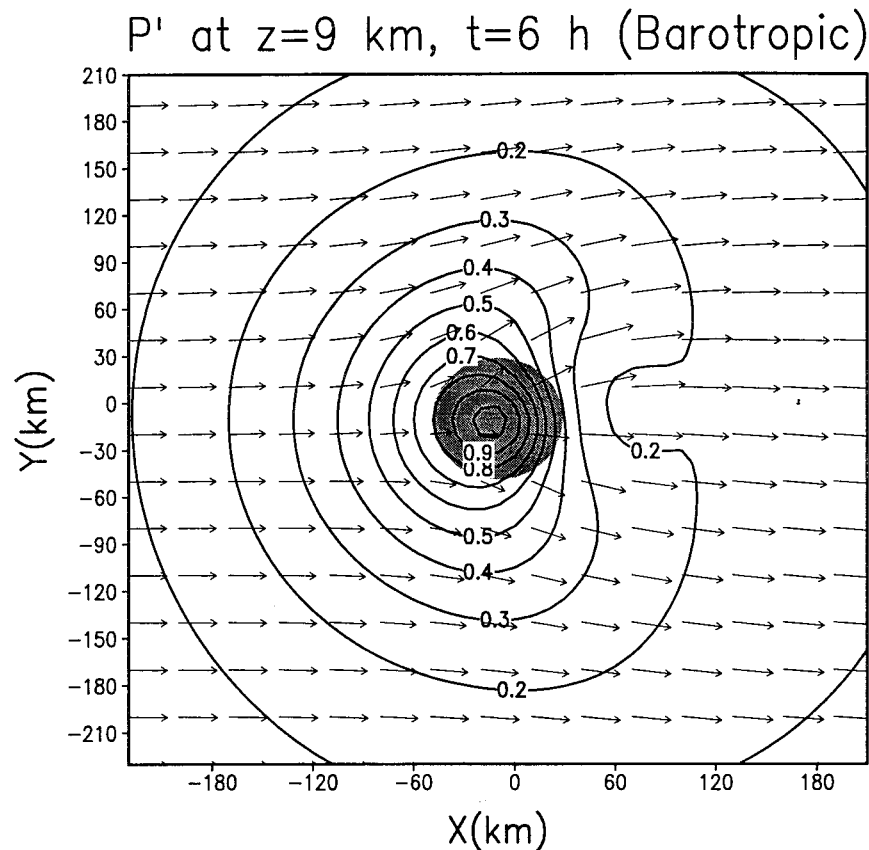


FIG. 7. Pressure perturbation (mb) and total horizontal wind vectors at $z = 9$ km and $t = 6$ h for the barotropic case.

ing region is clearly evident at $x = 0$ km. In Fig. 10a, the vertical velocity field clearly shows the stationary mode (solid phase line), which is delineated by the peak updraft that is maintained at $x = 0$ km throughout the simulation. After 6 h, wing patterns (dashed phase lines in Fig. 10a) reveal the lateral propagation of the dominant or “startup” wave that was initiated by the peak heating pulse. The eastward tilting of the wing pattern is due to the advection of the propagating wave mode by the basic state wind. By 8 h, the bifurcation of the zonal wind maximum (Fig. 10b) is apparent at $x = 40$ km, which is associated with the propagating mode. The zonal wind maximum, as well as the pressure and potential temperature perturbations associated with the mesocyclone, propagates downstream at a speed of 11 m s^{-1} and is delineated by the phase lines (dashed) in Figs. 10b–d, respectively.

A scaling parameter that addresses mass momentum adjustments is the Rossby radius of deformation (e.g., Blumen 1972; Frank 1983),

$$\lambda_R = \frac{NH}{(\zeta + f)^{1/2}(2VR^{-1} + f)^{1/2}}, \quad (4)$$

where

N = Brunt–Väisälä frequency,

H = scale depth of the disturbance,

ζ = the vertical component of relative vorticity,

f = the Coriolis parameter, and

V = the tangential component of the wind at the radius of curvature R .

This parameter, λ_R , is a crude scaling for determining the importance of rotational influences on a convective system. If the scale of the disturbance exceeds λ_R , the circulation can become geostrophically balanced, and the wind field will adjust to the mass perturbation generated by convection. On the other hand, if the scale of the disturbance is smaller than λ_R , the mass field adjusts to the wind field, the system will not attain geostrophic balance, and the energy released by convective latent heating will generate gravity waves that disperse the energy both horizontally and vertically.

Figures 11a and 11b reveal the 5-km perturbation and total wind velocity magnitudes and vector fields for the barotropic case, respectively. It is clearly evident in Fig. 11b that the addition of the basic-state wind yields a midlevel isotach maximum of 12.5 m s^{-1} to the south of the heating. Calculation of Eq. (4) at 12 h reveals that λ_R is larger than the scale of the mesoscale cyclone, based on the following parameters: $H = 10$ km, ζ ($z = 5$ km) = $1.2 \times 10^{-4} \text{ s}^{-1}$, $R = 50$ km, and V ($R = 50$

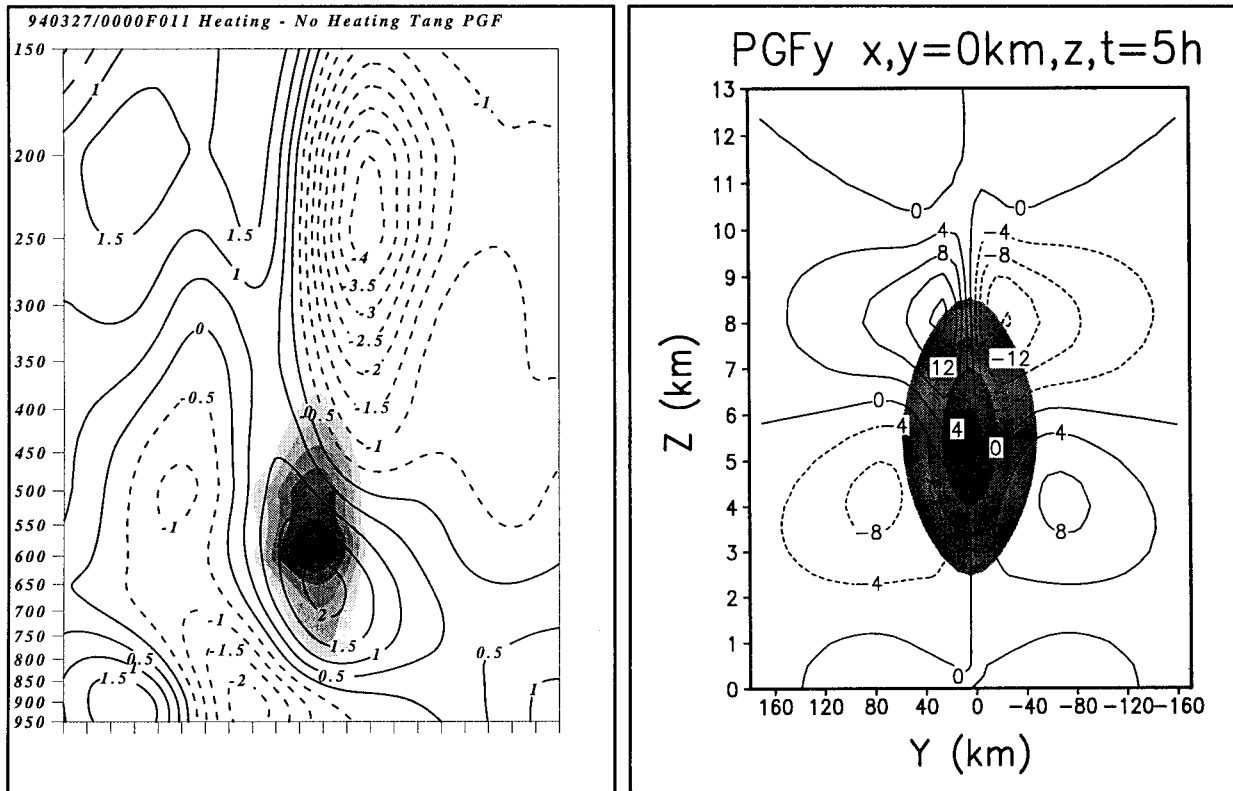


FIG. 8. Vertical cross sections of the (a) MASS heating–no heating difference in the pressure gradient force tangential to the plane (grid interval = 24 km) and (b) the GFDM pressure gradient force. Cross sections are oriented north–south and normal to the basic flow. Shaded region represents heating at $1 \text{ K (30 min)}^{-1}$ intervals.

km) = 3 m s^{-1} . Therefore, since $\lambda_R = 500 \text{ km}$ and the scale of the disturbance is on the order of 100 km, the mass perturbations should adjust to the wind perturbations. This appears to be the case as a 5-km warm core develops at 10 h (Fig. 9c), 2 h after identification of the 5-km perturbation mesocyclone (Fig. 9a). This phase lag of low pressure and warm core development is also evident in Fig. 10c and 10d.

At 9 km, a meso- β -scale anticyclone aloft attends the midlevel mesoscale cyclone, and attains a localized wind maximum on the left-forward flank of the heating region (Fig. 9c). This feature is consistent with the findings of Maddox (1979). This mesoscale anticyclone slowly decays as it advects downstream.

d. Comparison of MASS and GFDM barotropic jetlets

The vertical structure of the local wind maximum is examined. Cross-stream vertical cross sections detail the influence of the local wind maximum on the surrounding environment. In particular, to be addressed here is an analysis of the local wind maximum's associated transverse vertical circulations. Recalling the discussion from the previous section, where the vertical circulations about the downstream propagating midlevel jetlet sim-

ulated by MASS rendered a thermally direct (indirect) circulation below (above) the level of maximum winds (to be referred as the “circulation couplet”), we now examine the transverse flow about the local wind maximum simulated by the idealized experiment. At 6 h, similar features exist, but are not well defined. In fact, it appears that the circulations at this time are primarily forced by compensating motions triggered by the thermally forced gravity wave that continuously grows with time as the heating is increased. By 9 h, a distinct circulation couplet has developed (Figs. 12a and 12b). At midlevels ($z = 6 \text{ km}$), strong ascent is forced at the center of the heating ($y = 0 \text{ km}$), while midlevel compensating downward motion is apparent to the south of the origin ($y = -200 \text{ km}$). Conversely, at lower levels ($z < 2 \text{ km}$), downward motion below the heat source is compensated to the south with upward motion. This flow structure is consistent with the circulations found in the MASS simulation (Figs. 3a–c). This circulation couplet is apparent from the origin ($x = 0 \text{ km}$) to about 120 km downstream of the heating region. By 11 h, the circulation couplet has weakened and begins to propagate southward (Figs. 12c and 12d). This propagation is consistent with the dominant wave mode that was achieved by 6 h, which was then allowed to freely propagate away from the heating origin. The forced and

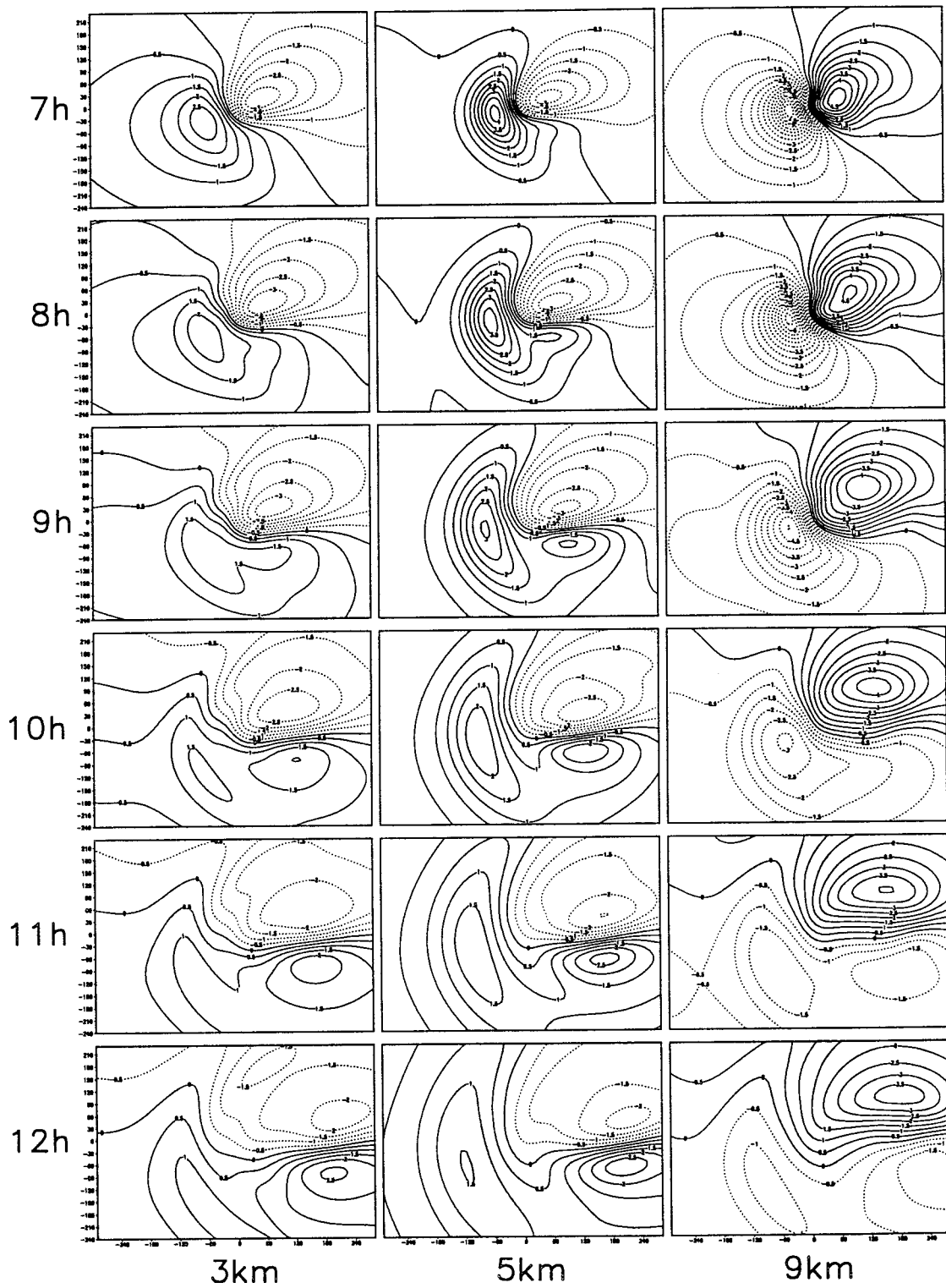


FIG. 9. Time evolution at 3, 5, and 9 km for the time period 7–12 h at 1-h increments for (a) u' , (b) p' , and (c) θ' .

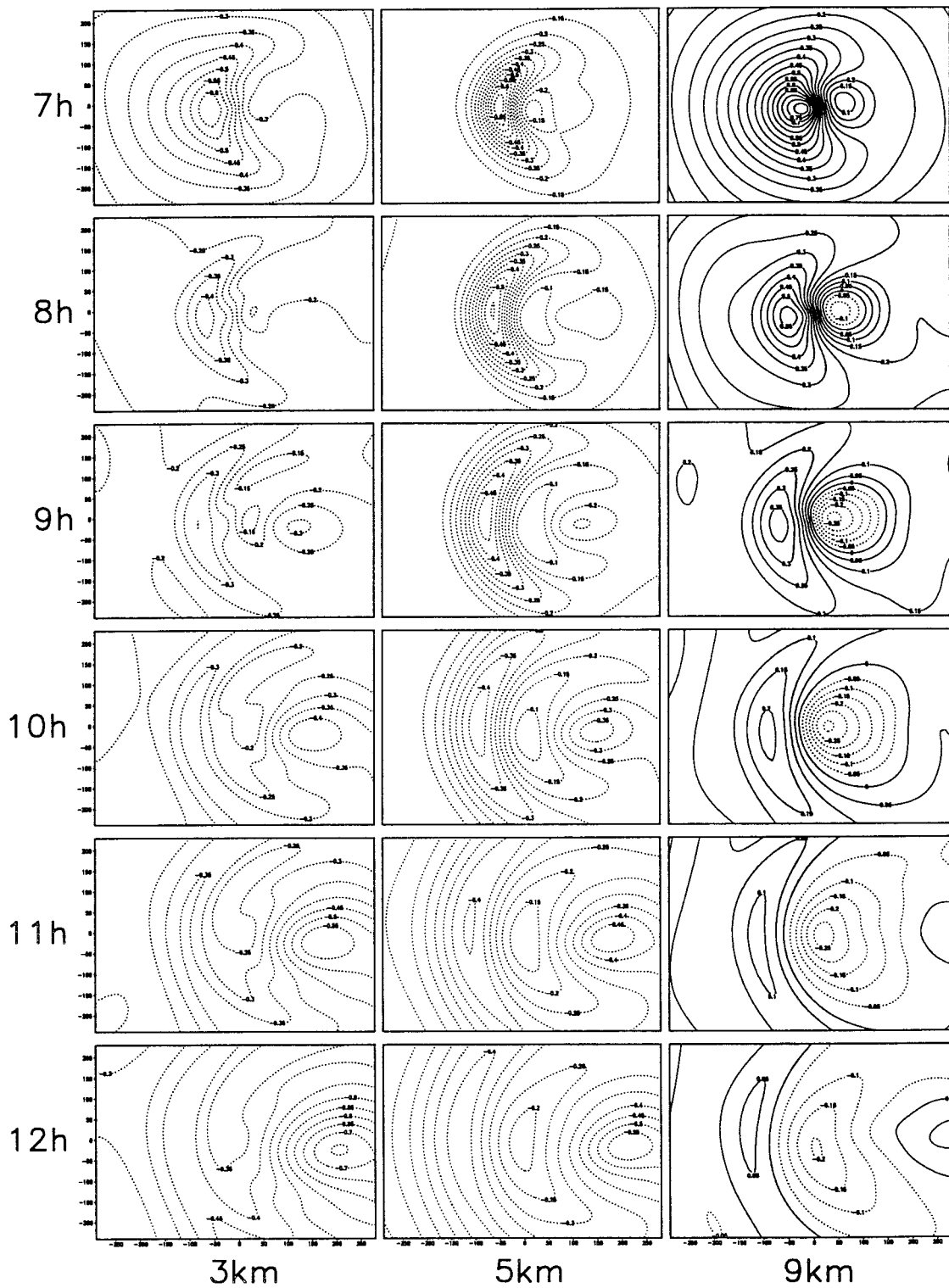


FIG. 9. (Continued)

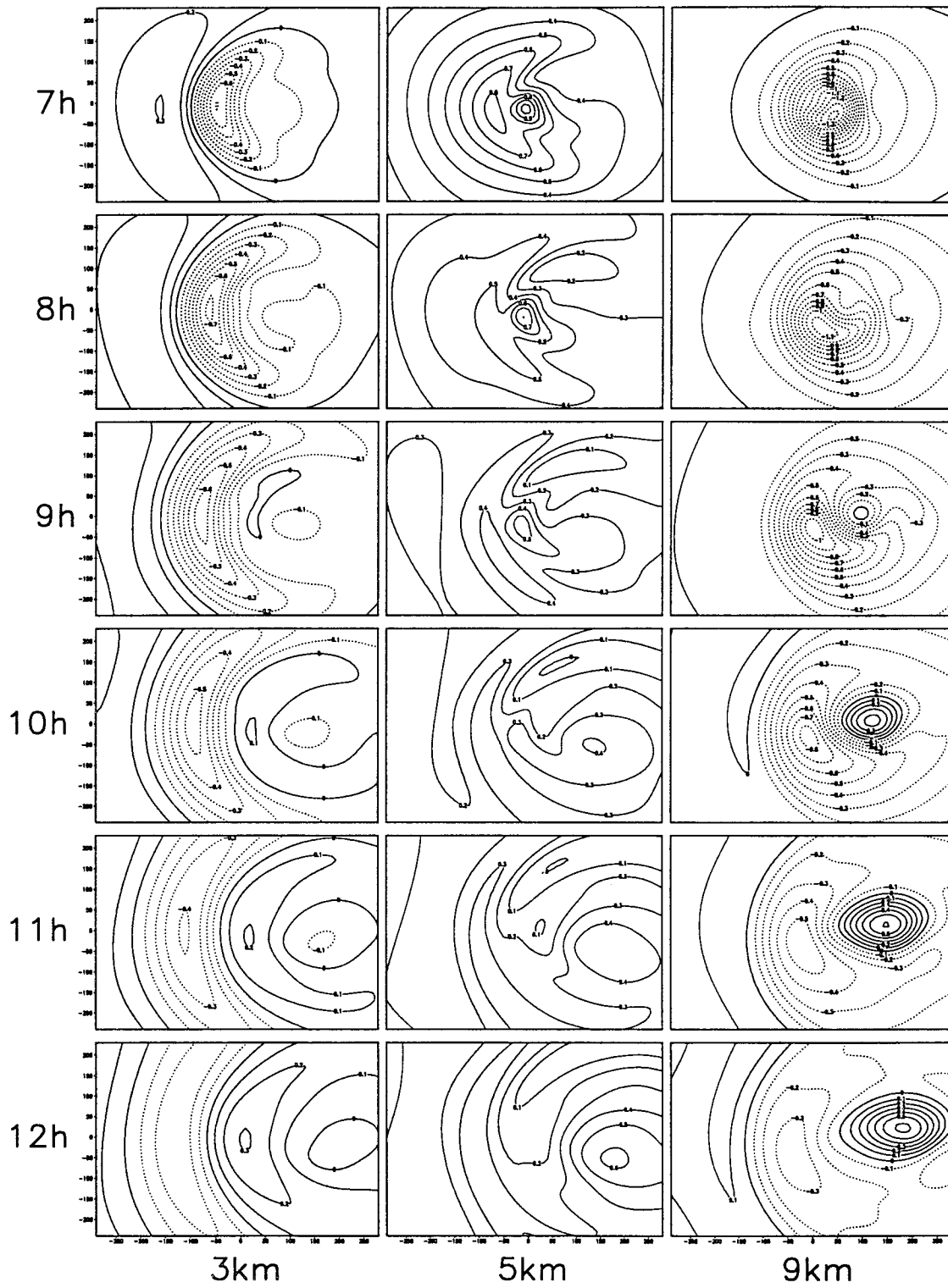


FIG. 9. (Continued)

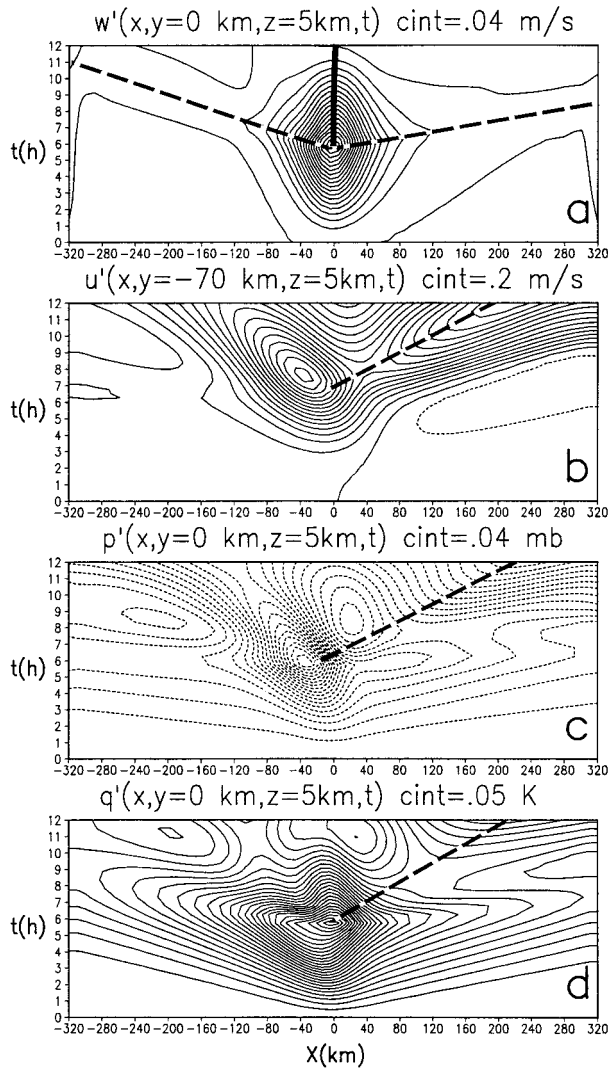


FIG. 10. Time–height cross sections at 5 km for (a) vertical velocity, (b) zonal wind perturbation, (c) pressure perturbation, and (d) potential temperature perturbation. Cross sections are oriented east–west through the center of heating.

compensating motions, associated with the dominant wave mode, allow the circulation couplet to freely disperse away from the heat source as the heating is decreased. The feature has completely dispersed by 12 h.

In summary, the application of a prescribed time-dependent heat source to a uniform continuously stratified flow can reveal the observed features of MCSs, and *does validate the hypothesis of the development of a midlevel local wind maximum, which is later found to propagate downstream as the heating is decreased.* From the comparison between the simple model results and the MASS results, the midlevel local wind maximum is part of the wind field associated with the development of a mesoscale perturbation cyclone simulated by GFDM, as opposed to the isolated midlevel jetlet simulated by MASS. A key similarity between the

MASS and GFDM results is the development of a vertical circulation couplet, which favors relatively weak ascending motion below and on the right flank of the midlevel local wind maximum.

e. Response of a continuously stratified baroclinic flow

The second case examines the response of a sheared environment and accompanying north–south basic-state potential temperature gradient, as required by thermal wind balance, to the thermal forcing. The shear flow is linear with form:

$$U(z) = -U_o + \left(\frac{U_o}{z_c}\right)z, \quad \text{for } U_o, z_c > 0, \quad (5)$$

where

$U(z)$ = basic zonal wind profile,

U_o = zonal basic wind at the surface, and

z_c = critical level or reversal height of the basic wind.

In the shear case $U_o = 6 \text{ m s}^{-1}$ and $z_c = 3 \text{ km}$. The shear is linear with height, with easterly flow in the lower levels and westerly flow aloft. The storm motion for the simulated convection in the MASS model run is $\sim 30 \text{ m s}^{-1}$, and has been subtracted out of the profile to examine the response from a storm-relative frame of reference. Therefore, a critical level is introduced at $z = 3 \text{ km}$. From Eq. (5), it can be seen that the zonal flow is unidirectional in the vertical, and has no horizontal shear.

The most notable feature for this case is the development of a strong midlevel cyclonic rotation around the heating region that propagates downstream after the maximum heating is achieved, similar to the midlevel mesoscale cyclone produced in the uniform flow case. In this case, however, the mesoscale cyclone is very distinct and reveals a closed circulation in the total wind field by the end of the simulation.

At 6 h, the 1-km vertical velocity field details the feature necessary for the maintenance of long-lived, deep convection (Fig. 13a). There exists weak upward motion at the heating base. Moving aloft, the vertical velocity field exhibits a fairly axisymmetric response at both 3 and 5 km, thus maintaining the organized updraft. At 9 h (Fig. 13b), the intrusion of a downdraft just downstream of the heating is apparent. At 13 h (Fig. 13c) a weak vertically propagating gravity wave is evident, indicated by the presence of the V-shaped signature with the vertex pointing upstream above the thermal forcing.

At 6 h, the 500-m horizontal wind fields (Fig. 14a) reveal a pattern of convergence similar to that found in the uniform case (Fig. 6a). At 5 km (Fig. 14b), positive u' component perturbations appear to be wrapping around the prescribed heat source. In a simulation with-

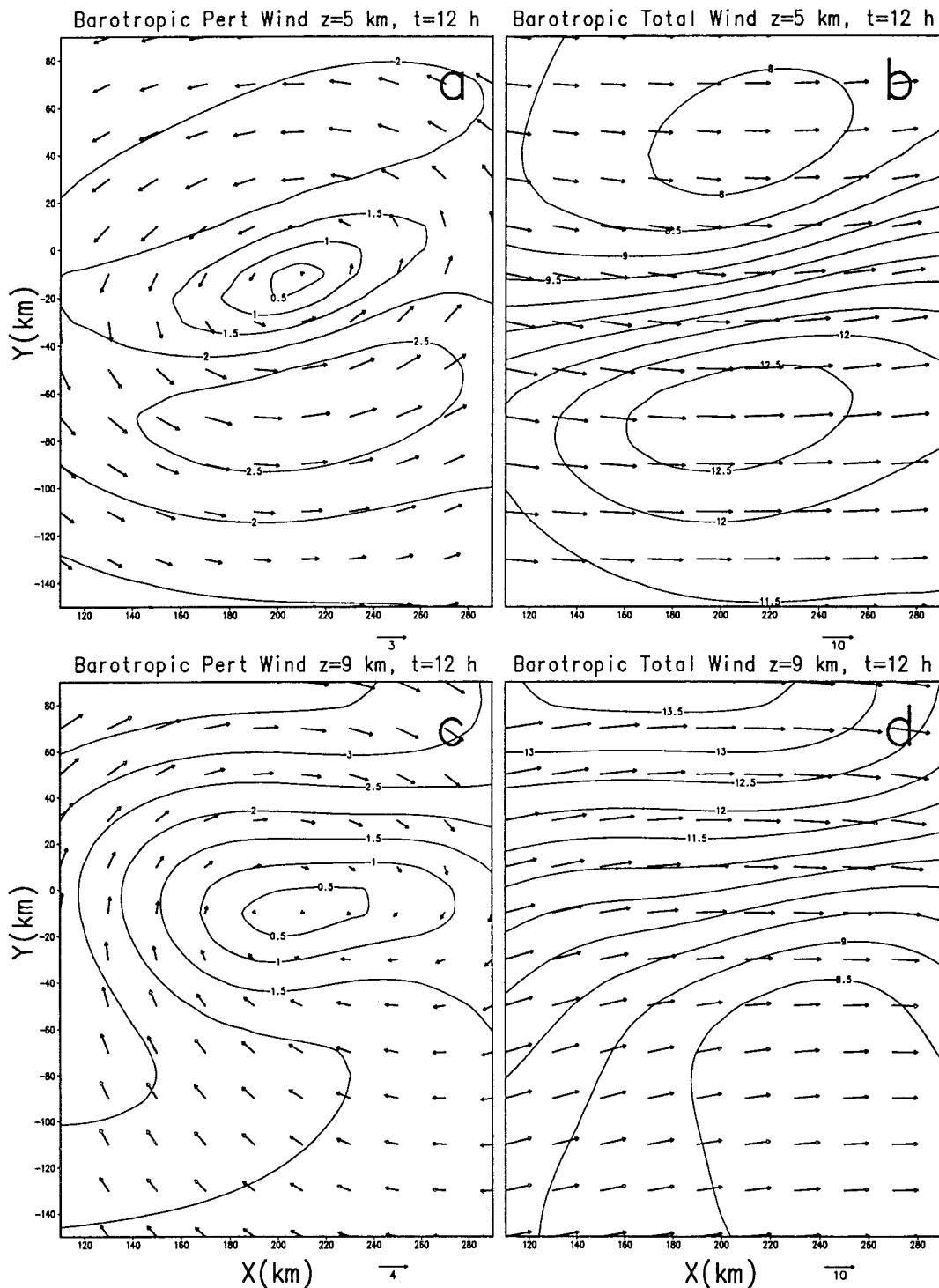


FIG. 11. (a) and (c) Perturbation and (b) and (d) total horizontal wind vectors and isotachs for the barotropic case at $t = 12$ h and (a) and (b) $z = 5$ km and (c) and (d) $z = 9$ km.

out the model's rotation, the enhanced zonal wind perturbations are of equal magnitude and symmetric about the x axis. In this case, where the rotation effect has been applied, a right flanking perturbation (~ 2 m s^{-1})

is wrapping around the southern region of the forcing and is of greater magnitude than the region wrapping around to the north. Embedded within the thermally forced region is a negative u' counter flow, which ex-

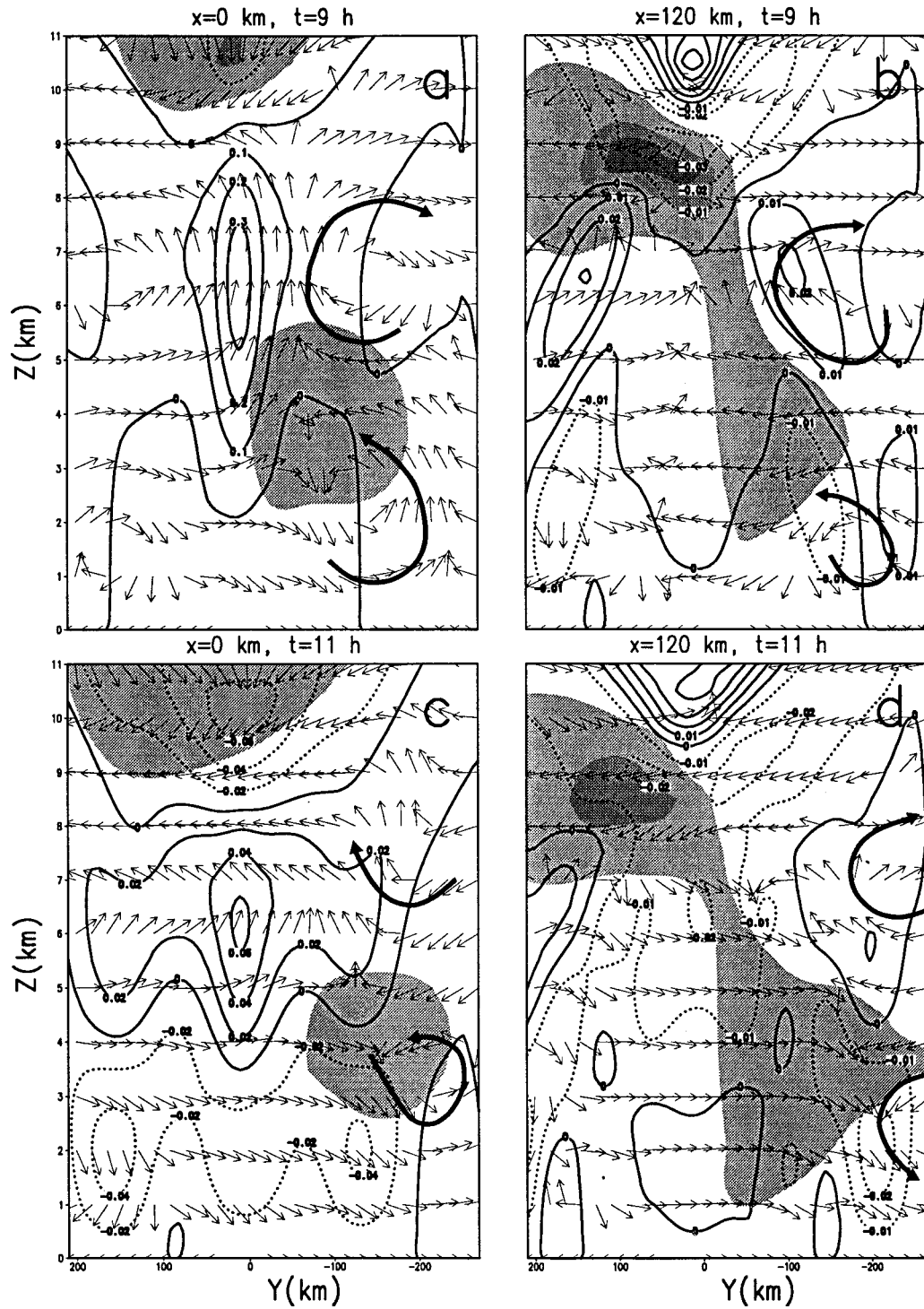


FIG. 12. Cross-stream vertical cross sections depicting the perturbation transverse circulation vectors and vertical velocity [solid (upward) and dotted (downward) lines] for the barotropic case. (a) and (b) The 9-h response at $x = 0$ and 120 km, respectively. (c) and (d) The 11-h response at $x = 0$ and 120 km, respectively. Positive u' values $> 1 \text{ m s}^{-1}$ are shaded at 1 m s^{-1} intervals.

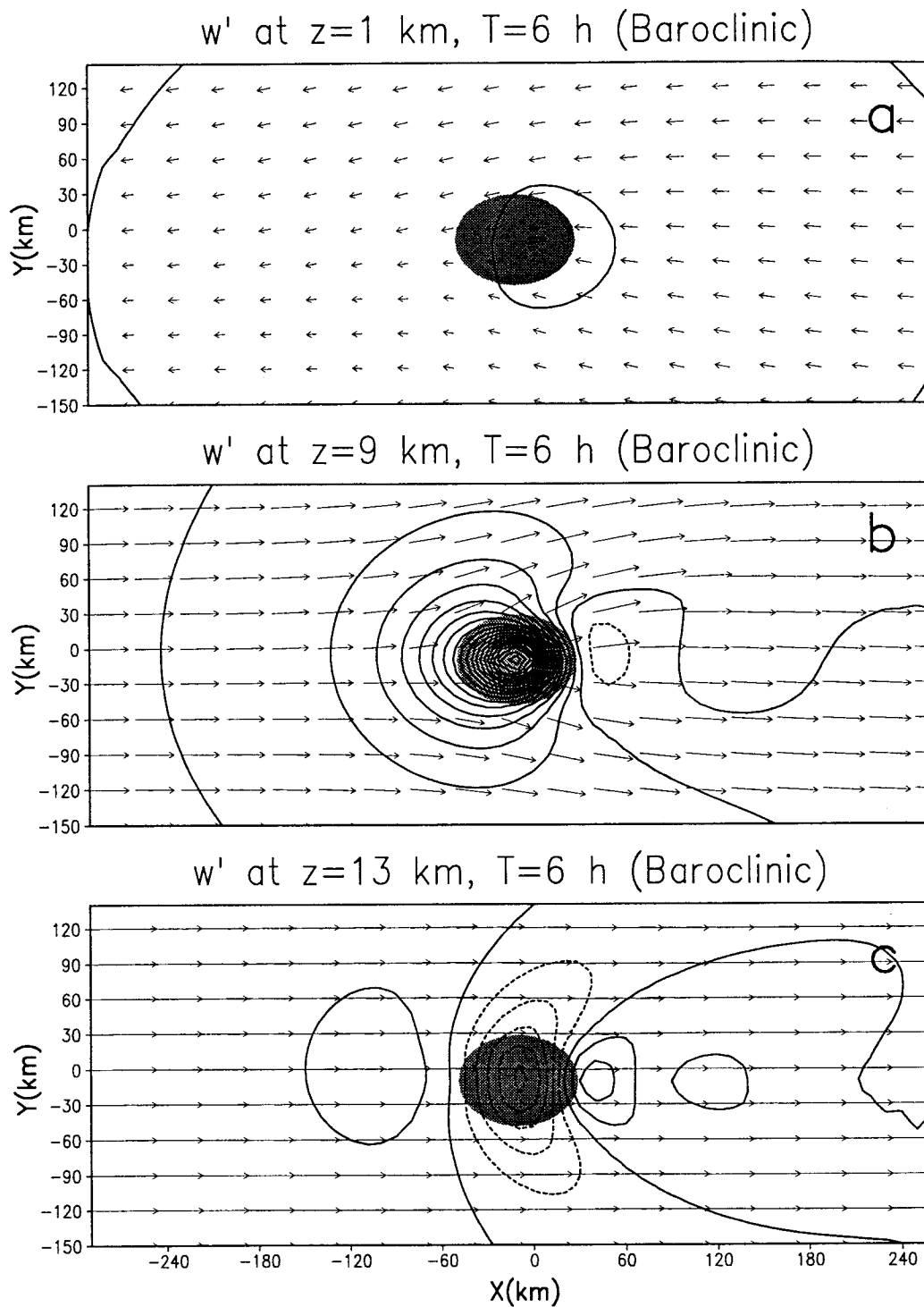


FIG. 13. Same as Fig. 5 except for baroclinic case.

tends downstream. At both 3 and 5 km, the v' fields also exhibit convergence, with a northerly perturbation component of over 3 m s^{-1} feeding the updraft core (not shown). At 9 km (Fig. 14c), divergence is apparent with

the downstream wind maximum developing on the left-forward flank of the heating region.

The midlevel zonal wind perturbation field, from 6 to 12 h, particularly at 5 km, exhibits a closed cir-

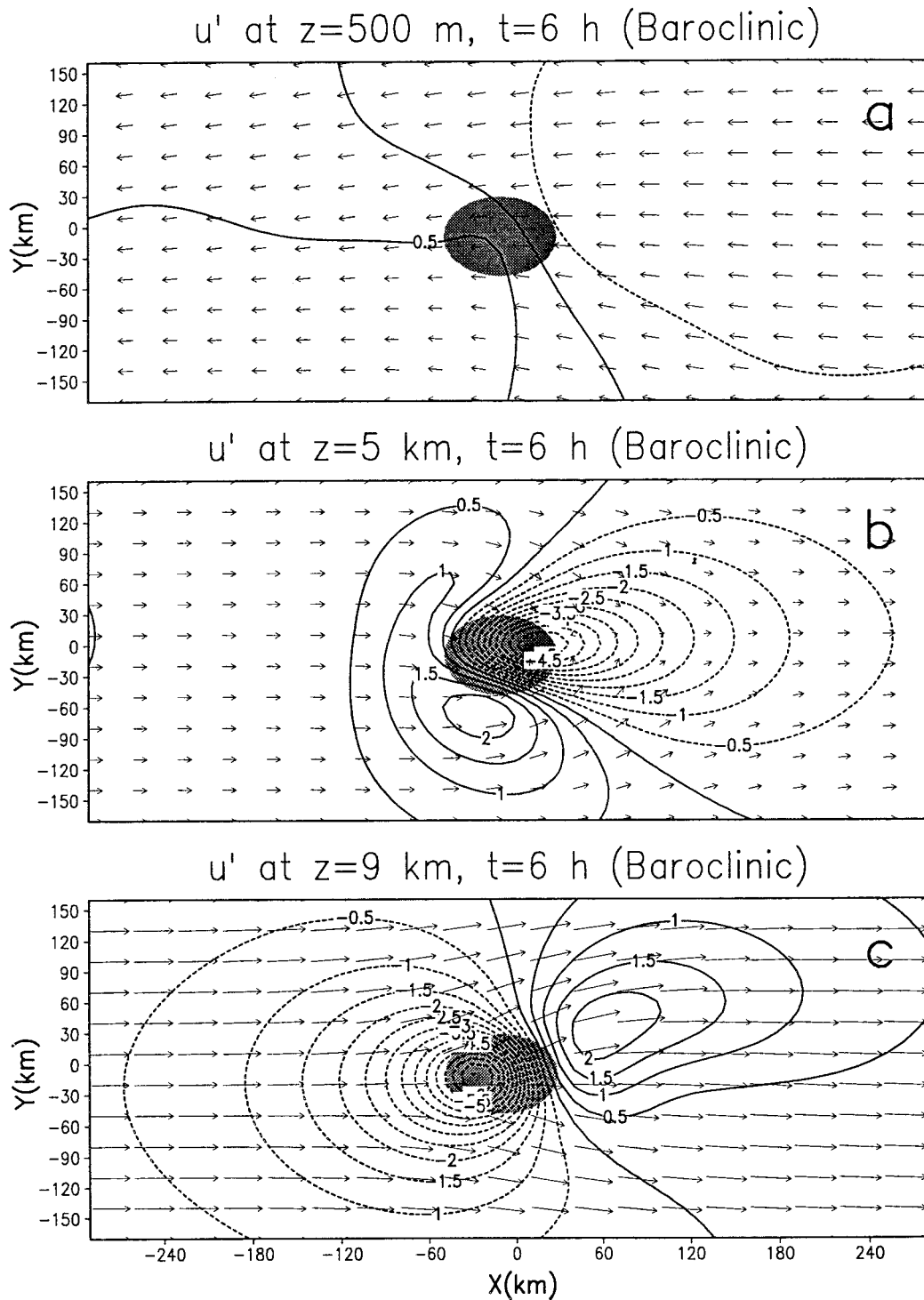


FIG. 14. Same as Fig. 6 except for baroclinic case.

lation, a perturbation low pressure center, and a warm core that develops and intensifies in the latter hours of the simulation. The closed circulation is similar to the formation of the mesoscale cyclone in the previous section and attains a total wind maximum ($\sim 7.5 \text{ m s}^{-1}$) on

the right flank of the circulation (Fig. 15b). Figures 15a and 15b reveal the 5-km perturbation and total wind velocity magnitudes and vectors for the baroclinic case, respectively. The parameters used in calculating the deformation radius λ_R are $H = 10 \text{ km}$, $\zeta (z = 5 \text{ km}) =$

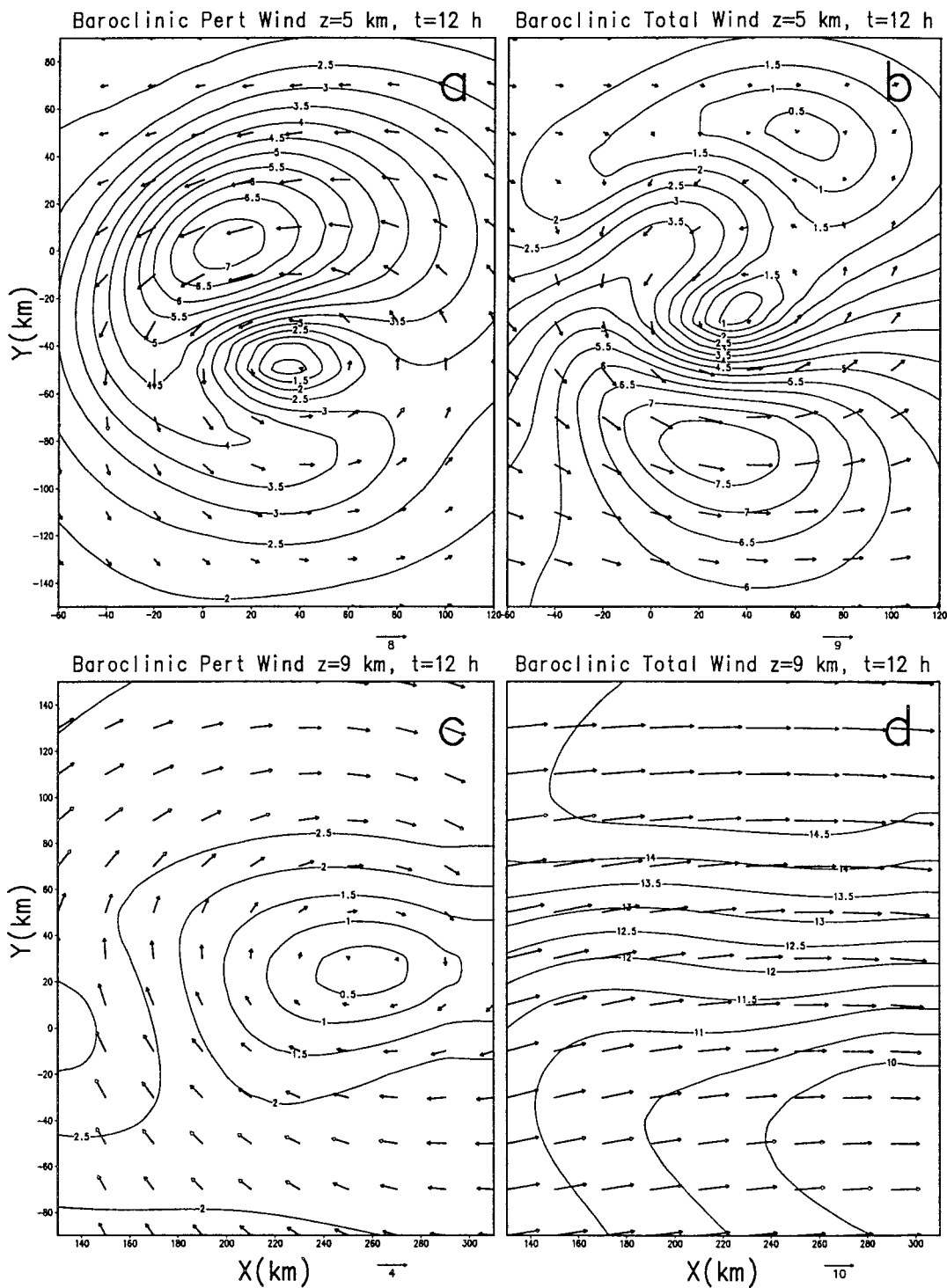


FIG. 15. Same as Fig. 11 except for baroclinic case. Note downstream displacement of 9-km fields.

$3.0 \times 10^{-4} \text{ s}^{-1}$, $R = 60 \text{ km}$, and $V(R = 60 \text{ km}) = 7 \text{ m s}^{-1}$. Now, $\lambda_R = 300 \text{ km}$ thus revealing a similar adjustment of the mesoscale cyclone produced in the shear flow case as compared to that produced in the uniform flow case of the previous section. In the final

6 h of the simulation, the mesoscale cyclone maintains constant wind velocities in the closed circulation while warming intensifies within the center of circulation (not shown). This indicates that the mass perturbations adjust to the wind perturbations.

The smaller magnitude of λ_R , in the baroclinic case, is attributed to the larger vorticity magnitude at mid-levels. As in the barotropic case, the closed circulation pattern strengthens as it propagates slowly downstream away from the heating origin during the later 6 h of the simulation. It should be noted that in the final 5 h of the simulation, the 5-km perturbation mesoscale cyclone propagates at nearly the speed of the mean wind (i.e., 4 m s^{-1}), but the pressure perturbation center propagates at more than half that speed (i.e., 1.5 m s^{-1}). Aloft, a reversed meso- β -scale anticyclonic circulation exists, but does not exhibit a closed circulation due to the stronger basic wind (Figs. 15d). Notice that Figs. 15c and 15d are displayed farther downstream than Figs. 15a and 15b, due to the faster upper-level advection associated with the vertical shear. Moreover, an enhanced wind maximum feature ($\sim 14.5 \text{ m s}^{-1}$) on the left flank of the diminished heating propagates downstream (Fig. 15d). This upper-level wind maximum is similar to the findings of Maddox (1979) and others.

f. Comparison of MASS and GFDM baroclinic jetlets

Once again an analysis of the local wind maximum's associated vertical circulations is addressed. As in the barotropic case, cross-stream vertical cross sections are examined. At 6 h, a distinct circulation is established between 3 and 8 km just to the south of the main updraft, but appears to be mainly driven by the prescribed heating (not shown). By 9 h, a circulation couplet has developed (Fig. 16a). The feature is displaced to the south of the midlevel local wind maximum and is consistent with the circulations found in MASS (Figs. 3a–c). This circulation couplet is apparent for about 40 km downstream. At $x = 80 \text{ km}$ (Fig. 16b), a similar flow structure is apparent, but the circulation is not well developed. At 11 h (Figs. 16c and 16d), the weakened circulation couplet is still evident and appears to be propagating southward away from the local wind maximum. Similar to the uniform flow case, the circulation couplet is attributed to the compensatory motions associated with the thermally forced gravity wave, which laterally disperses during the later stages of the simulation.

In summary, the application of a prescribed time-dependent heat source to a simple baroclinic shear flow can reproduce many of the observed characteristics of MCSs, and validates the hypothesis of the development of a mid-level mesoscale cyclone, and attending right flank local wind maximum, which is later found to propagate downstream as the heating is decreased. The prescribed basic shear flow differentially advects the local wind maximum, thus resulting in downshear tilting of the isotachs. The wind maximum, associated with the development of a meso- β -scale cyclone, does not appear to become an isolated jetlet feature like the one simulated by MASS. On the other hand, the baroclinic case does exhibit a larger zonal perturbation than the wind maximum in the barotropic case ($\sim 4 \text{ m s}^{-1}$ vs 3 m s^{-1}).

In reference to the hypothesis, nearly identical conclusions are made for this case as in the barotropic case. The major difference is that the vertical circulation couplet in the baroclinic case is not as well defined as the one found in the barotropic case, but is found to favor ascent below and to the south of the midlevel local wind maximum. This is supportive of the dynamics established by the MASS model.

4. Summary

A primitive equation model with a prescribed thermal forcing has been implemented to examine the development of the right flank midlevel jetlet. The thermal forcing is used to replicate and isolate the effects of latent heat release in the MASS simulated mesoscale convective system so that the complex adjustments can be more easily comprehended. Since only small variations in the barotropic and baroclinic cases were found in the idealized experiments, the attending mass-momentum adjustments to the prescribed thermal forcing of both flows can be consolidated and summarized in the following manner.

The results confirm that latent heating alone plays an important role in the development of a midlevel right flank wind maximum that is associated with the formation of a midlevel meso- β -scale cyclone. Maximum heating around the midtroposphere (e.g., 5.5 km) triggers consecutive pressure falls and rises, below and above the level of maximum heating, respectively. Therefore, below the level of maximum heating, a continuous geostrophic adjustment of the winds occurs as air parcels accelerate toward the heating center due to the increase in the pressure gradient force. Rotational forces subsequently act to turn the air parcels to the right, thus leading to the development of vertical vorticity. Enhanced convergence into the heating region drives ascent, due to mass continuity, leading to column stretching and the intensification of cyclonic vorticity just below the level of maximum heating. In both barotropic and baroclinic cases, the addition of the basic-state flow to the perturbations at this level yields the right-flanking wind maximum. Conversely, at upper levels where pressure rises are experienced, geostrophic adjustment leads to an anticyclonic circulation aloft and a left forward-flank wind maximum, which is consistent with previous observational and modeling studies.

As the disturbance intensifies and midlevel vorticity increases, the Rossby radius of deformation decreases, though it remains larger than the scale of the disturbance. In agreement with theory, adjustment of the mass perturbations to the wind perturbations reveal the subsequent development of both a midlevel warm core and a low pressure center that intensify with time as the perturbation midlevel mesocyclone propagates downstream.

The effects of transient heating, where the heating is allowed to increase and then decrease with time, appears important for allowing the marked appearance of the

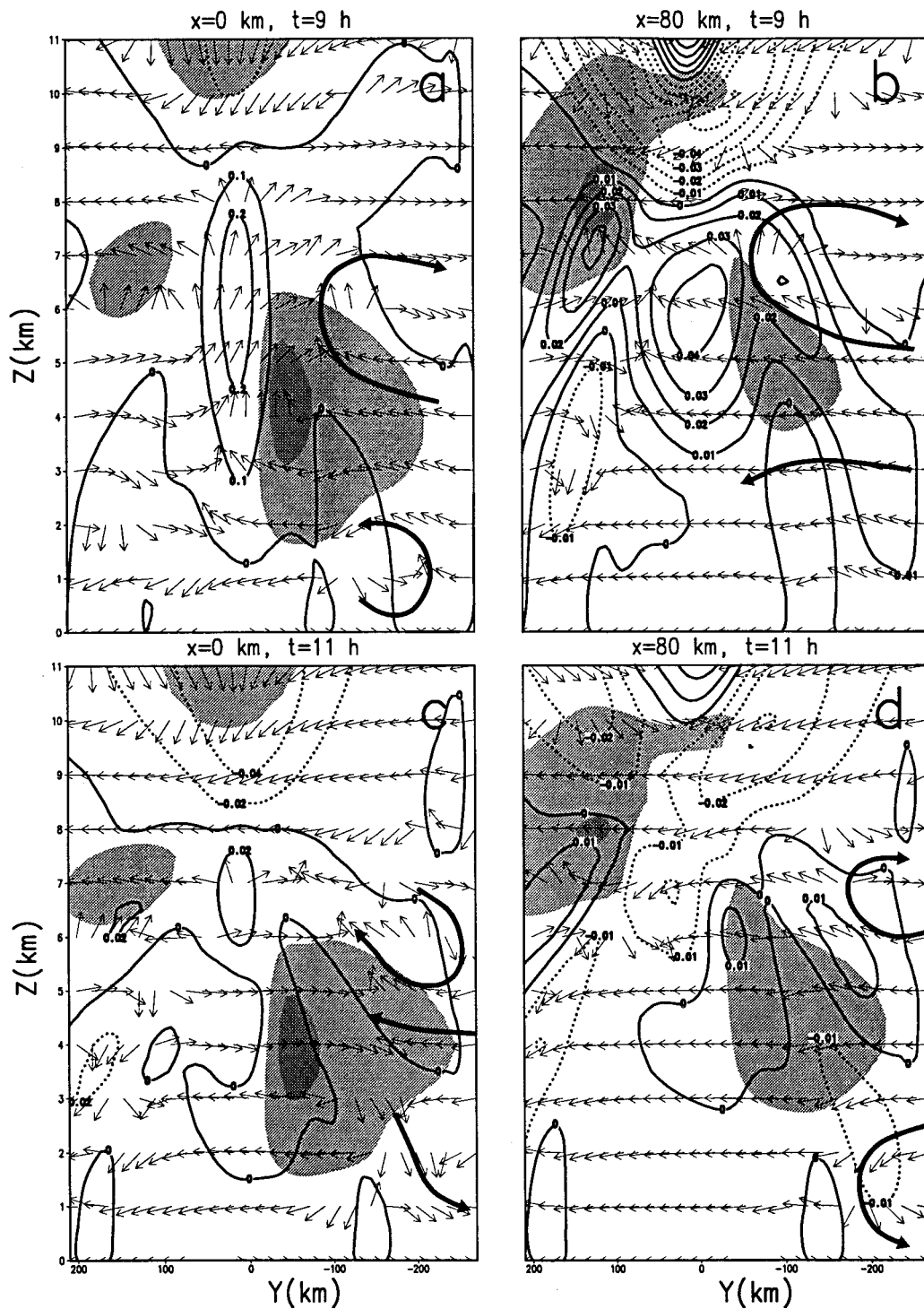


FIG. 16. Same as in Fig. 12 except for the baroclinic case and (b) and (d) are at $x = 80$ km.

downstream propagating midlevel mesoscale cyclone and the attending local wind maximum. The difference between the cases presented is that in the baroclinic case the advective response to the sheared flow is to differentially advect the local wind maximum structure. Thus

the disturbance is tilted downshear. From the first conclusion, it is speculated that if the perturbation midlevel mesoscale cyclone was allowed to persist further than the prescribed 12-h simulation, the disturbance would release energy in the form of gravity waves and would

eventually disperse, but is left open for further investigation.

Also, compensatory motions produced by the development of thermally forced vertically propagating gravity waves may aid in the development of a transverse vertical circulation couplet. This couplet could possibly trigger and/or maintain convection further downstream. The formation and propagation of these gravity waves are consistent with past studies (e.g., Lin 1986). Vertical shear allows for differential wave propagation throughout the depth of the column, therefore, somewhat masking the development of the wave at levels where the basic flow is nearly quiescent; that is, near the critical level. Moreover, the wave is allowed to rapidly propagate away from the region of wave generation.

The three-dimensional responses of both simple uniform and shear flows to a prescribed diabatic forcing have aided in the understanding of midlevel atmospheric responses to the latent heat release in a mesoscale convective system. The results used to explain the more complex results from the full physical simulation (MASS) of the 1994 Palm Sunday tornado outbreak reveal the importance of idealized numerical simulations in studying atmospheric phenomena such as deep convection. From these experiments, it appears that the diabatic forcing prescribed in the GFDM model validly simulates the observed features of mesoscale convection. On the other hand, the trend of simulated latent heat release in the MASS model is difficult to isolate due to the multicellular nature of the model convection. It appears crucial that the constant triggering of convection by MASS is additive in quantity and leads to a continuous geostrophic adjustment and hence a stronger, more isolated jetlet. Furthermore, presence of a three-dimensional horizontally and vertically sheared baroclinic state and a background pressure gradient field in MASS may contribute to a difference in the handling of the adjustment process that leads to jetlet formation. Finally, the obvious sophistication of cloud-physical processes demonstrated by MASS plays an important role in the convective feedback to the ambient environment. A similar type of feedback cannot be represented by GFDM due to the simple model formulation. Moreover, the mesoscale circulations in MASS can directly influence the background synoptic-scale flow, whereas the background basic-state thermal wind balance in GFDM is time independent and unchanged by the developing perturbations. Though the perturbation wind maximum feature simulated by GFDM and the jetlet simulated by MASS differ, it is noted that the wind velocity, at the level of maximum velocity perturbation, does significantly increase. As was described in the above analysis of the GFDM results, maximum wind velocity of the total zonal flow increases by nearly 25% in the barotropic case and 45% in the baroclinic case. This increase is nearly equal to that of the velocity increases in MASS, from 35 m s^{-1} to 50 m s^{-1} , and thus is supportive of the dynamics established by the MASS

model. Extension of the simple model should be made to include a more realistic heating parameterization, such as a wave-CISK mechanism, and three-dimensional wind shear. However, the present study provides valuable explanations of midlevel mass-momentum adjustments to latent heat release in a hydrostatic airflow.

Acknowledgments. The authors have benefited considerably from the comments of Drs. S. E. Koch and A. J. Riordan. This work has been supported by Air Force Grant F49620-95-1-0226, NSF Grant ATM-9224595, as well as NOAA Grant NA27RP029201 as part of the Southeast Consortium on Severe Thunderstorms and Tornadoes. Part of the computations were performed on IBM workstations, which are part of the FOAM^v computing facility at NCSU, and the supercomputer at the North Carolina Supercomputing Center.

REFERENCES

- Anthes, R. A., Y.-H. Kuo, S. G. Benjamin, and Y.-F. Li, 1982: The evolution of the mesoscale environment of severe local storms: Preliminary modeling results. *Mon. Wea. Rev.*, **110**, 1187–1213.
- Bluestein, H. B., and K. W. Thomas, 1984: Diagnosis of a jet streak in the vicinity of a severe weather outbreak in the Texas panhandle. *Mon. Wea. Rev.*, **112**, 2499–2520.
- Blumen, W., 1972: Geostrophic adjustment. *Rev. Geophys. Space Phys.*, **10**, 485–528.
- Bretherton, C., 1988: Group velocity and the linear response of stratified fluids to internal heat or mass sources. *J. Atmos. Sci.*, **45**, 81–93.
- Cotton, W. R., and R. A. Anthes, 1989: *Storm and Cloud Dynamics*. Academic Press, 883 pp.
- , M.-S. Lin, R. L. McAnelly, and C. J. Tremback, 1989: A composite model of mesoscale convective complexes. *Mon. Wea. Rev.*, **117**, 765–783.
- Fankhauser, J. C., 1971: Thunderstorm–environment interactions determined from aircraft and radar observations. *Mon. Wea. Rev.*, **99**, 171–192.
- Frank, W. M., 1983: The cumulus parameterization problem. *Mon. Wea. Rev.*, **111**, 1859–1871.
- Fujita, T., 1982: Principle of stereographic height computations and their applications to stratospheric cirrus over severe thunderstorms. *J. Meteor. Soc. Japan*, **60**, 355–368.
- Hales, J. E., and M. D. Vescio, 1996: The March 1994 tornado outbreak in the southeast U. S: The forecast process from an SPC perspective. Preprints, *18th Conf. on Severe Local Storms*, San Francisco, CA, Amer. Meteor. Soc., 32–36.
- Heymsfield, G. M., R. H. Blackmer Jr., and S. Schotz, 1983: Upper-level structure of Oklahoma tornadic storms on 2 May 1979: Part I. *J. Atmos. Sci.*, **40**, 1740–1755.
- Kaplan, M. L., J. W. Zack, V. C. Wong, and J. J. Tuccillo, 1982: Initial results from a Mesoscale Atmospheric Simulation System and comparisons with the AVE-SESAME I data set. *Mon. Wea. Rev.*, **110**, 1564–1590.
- , Y.-L. Lin, D. W. Hamilton, and R. A. Rozumalski, 1996: The numerical simulation of an unbalanced jetlet and its role in the Palm Sunday 1994 tornado outbreak in Alabama and Georgia. Preprints, *18th Conf. on Severe Local Storms*, San Francisco, CA, Amer. Meteor. Soc., 240–244.
- , —, —, and —, 1998: The numerical simulation of an unbalanced jetlet and its role in the Palm Sunday 1994 tornado outbreak in Alabama and Georgia. *Mon. Wea. Rev.*, **126**, 2133–2165.
- Koch, S. E., Y.-L. Lin, M. L. Kaplan, M. Vescio, A. Langmaid, D. W. Hamilton, D. Kramer, and M. Black, 1996: Frontal mesolow

- dynamics in the Palm Sunday tornado outbreak. Preprints, *18th Conf. on Severe Local Storms*, San Francisco, CA, Amer. Meteor. Soc., 47–51.
- Lin, Y.-L., 1986: Calculation of airflow over an isolated heat source with application to the dynamics of V-shaped clouds. *J. Atmos. Sci.*, **43**, 2736–2751.
- , and R. B. Smith, 1986: Transient dynamics of airflow near a local heat source. *J. Atmos. Sci.*, **43**, 40–49.
- , and S. Li, 1988: Three-dimensional response of a shear flow to elevated heating. *J. Atmos. Sci.*, **45**, 2987–3002.
- , and I.-C. Jao, 1995: A numerical study of flow circulations in the Central Valley of California and formation mechanisms of the Fresno eddy. *Mon. Wea. Rev.*, **123**, 3227–3239.
- Maddox, R. A., 1979: The evolution of middle and upper tropospheric features during a period of intense convective storms. Preprints, *11th Conf. on Severe Local Storms*, Kansas City, KS, Amer. Meteor. Soc., 41–48.
- , D. J. Perkey, and J. M. Fritsch, 1981: Evolution of upper tropospheric features during the development of a mesoscale convective complex. *J. Atmos. Sci.*, **38**, 1664–1674.
- Raymond, D. J., 1976: Wave-CISK and convective mesosystems. *J. Atmos. Sci.*, **33**, 2392–2398.
- Smith, R. B., 1980: Linear theory of stratified hydrostatic flow past an isolated mountain. *Tellus*, **32**, 348–364.
- Uccellini, L. W., and D. R. Johnson, 1979: The coupling of upper- and lower-tropospheric jet streaks and implications for the development of severe convective storms. *Mon. Wea. Rev.*, **107**, 682–703.
- Wang, T.-A., Y.-L. Lin, H. F. M. Semazzi, and G. S. Janowitz, 1996: Response of a stably stratified atmosphere to large-scale diabatic forcing with applications to wind patterns in Brazil and the Sahel. *J. Geophys. Res.*, **101**, 7049–7073.
- Weglarz, R. P., 1994: Three-dimensional geostrophic adjustment of homogeneous and continuously stratified atmospheres with application to the dynamics of midlatitude jet streaks. Ph.D. thesis, North Carolina State University, 414 pp.
- Wolf, B. J., and D. R. Johnson, 1995: The mesoscale forcing of a midlatitude upper-tropospheric jet streak by a simulated convective system. Part I: Mass circulation and ageostrophic processes. *Mon. Wea. Rev.*, **123**, 1059–1087.
- Zack, J. W., and M. L. Kaplan, 1987: Numerical simulations of the subsynoptic features associated with the AVE-SESAME I case. Part I: The preconvective environment. *Mon. Wea. Rev.*, **117**, 2067–2094.